Electronic Supplementary Information

New structural hypostasis of the A·T and G·C Watson-Crick DNA base pairs caused by their mutagenic tautomerisation in a wobble manner: A QM/QTAIM prediction

Ol'ha O. Brovarets'[a,b] & Dmytro M. Hovorun[a,b,✉]

[a]Department of Molecular and Quantum Biophysics, Institute of Molecular Biology and Genetics, National Academy of Sciences of Ukraine, 150 Akademika Zabolotnoho Str., 03680 Kyiv, Ukraine

[b]Department of Molecular Biotechnology and Bioinformatics, Institute of High Technologies, Taras Shevchenko National University of Kyiv, 2-h Akademika Hlushkova Ave., 03022 Kyiv, Ukraine

✉Corresponding author. E-mail: dhovorun@imbg.org.ua

1. Computational Details.

Density functional theory geometry and vibrational frequencies calculations. All calculations of the geometries and harmonic vibrational frequencies of the considered base mispairs and transition states of their conversion have been performed using Gaussian'09 package[1] at the DFT (B3LYP)/6-311++G(d,p) level of theory[2-4], that has been applied for analogous systems and verified to give accurate geometrical structures, normal mode frequencies, barrier heights and characteristics of intermolecular H-bonds[5,6]. A scaling factor that is equal to 0.9668 has been applied in the present work for the correction of the harmonic frequencies of all studied base pairs[7-9]. We have confirmed the minima and TSs, located by means of Synchronous Transit-guided Quasi-Newton method[10], on the potential energy landscape by the absence or presence, respectively, of the imaginary frequency in the vibrational spectra of the complexes. We applied standard TS theory[11] to estimate the activation barriers of the tautomerisation reaction.

Surrounding effects. In order to examine the surrounding effect on the considered tautomerisation processes, we have reoptimized geometries of the complexes at the B3LYP/6-311++G(d,p) level of theory using the commonly applied Conductor-Like Polarizable Continuum Model (CPCM)[12-14], choosing the continuum with a dielectric constant of ε=4 typical for the hydrophobic interiors of proteins[15] and for the hydrophobic interfaces of specific protein-nucleic acid interactions[16-20].

IRC calculations. Reaction pathways have been monitored by following intrinsic reaction coordinate (IRC) in the forward and reverse directions from each TS using Hessian-based predictor-corrector integration algorithm[21] with tight convergence criteria. These calculations eventually ensure that the proper reaction pathway, connecting the expected reactants and products on each side of the TS, has been found. We've have investigated the evolution of the energetic and geometric characteristics of the H-bonds and base pairs along the reaction pathway establishing them at each point of the IRC[22,23].

Single point energy calculations. In order to consider electronic correlation effects as accurately as possible, we followed geometry optimizations with single point (SP) energy calculations using MP2 level of theory[24] and 6-311++G(2df,pd) Pople's basis set of valence triple-ζ quality[25,26] and aug-cc-pVDZ Dunning's cc-type basis set[27], augmented with polarization and/or diffuse functions.

The Gibbs free energy G for all structures was obtained in the following way:

$$G=E_{el}+E_{corr}, \quad (1)$$

where E_{el} – electronic energy, while E_{corr} – thermal correction.

Evaluation of the interaction energies. Electronic interaction energies E_{int} have been calculated at the MP2/6-311++G(2df,pd) level of theory as the difference between the total energy of the base mispair and the energies of the isolated monomers. Gibbs free energy of interaction has been obtained using similar equation. In each case the interaction energy was corrected for the basis set superposition error (BSSE)[28,29] through the counterpoise procedure[30,31].

Estimation of kinetic parameters. The time $\tau_{99.9\%}$ necessary to reach 99.9% of the equilibrium concentration of the reactant and product in the system of reversible first-order forward (k_f) and reverse (k_r) reactions can be estimated by formula[11]:

$$\tau_{99.9\%} = \frac{ln10^3}{k_f + k_r}. \quad (2)$$

The lifetime τ of the wobble mismatches has been calculated using the formula $1/k_r$, where the values of the reverse k_r and forward k_f rate constants for the tautomerisation reactions were obtained as[11]:

$$k_{f,r} = \Gamma \cdot \frac{k_B T}{h} e^{-\frac{\Delta\Delta G_{f,r}}{RT}}, \quad (3)$$

where quantum tunneling effect are accounted by Wigner's tunneling correction[32], that has been successfully used for the DPT reactions[33,34]:

$$\Gamma = 1 + \frac{1}{24}\left(\frac{h\nu_i}{k_B T}\right)^2, \quad (4)$$

where k_B – Boltzmann's constant, h – Planck's constant, $\Delta\Delta G_{f,r}$ – Gibbs free energy of activation for the tautomerisation reaction in the forward (f) and reverse (r) directions, ν_i – magnitude of the imaginary frequency associated with the vibrational mode at the TSs.

QTAIM analysis. Bader's quantum theory of Atoms in Molecules (QTAIM) was applied to analyse the electron density distribution[35-38]. The topology of the electron density was analysed using program package AIMAll[39] with all default options. The presence of a bond critical point (BCP), namely the so-called (3,-1) BCP, and a bond path between hydrogen donor and acceptor, as well as the positive value of the Laplacian at this BCP ($\Delta\rho>0$), were considered as criteria for the H-bond formation[40,41]. Wave functions were obtained at the level of theory used for geometry optimisation.

Calculation of the energies of the intermolecular bonds. The energies of the AH···B H-bonds, including weak CH···O/N H-bonds[40-42], NH···HN dihydrogen bonds and attractive O/N···O/N van der Waals

contacts in the base mispairs and TSs of their interconversion and conventional H-bonds under the investigation of the sweeps of their energies were calculated by the empirical Espinosa-Molins-Lecomte (EML) formula[42-44] based on the electron density distribution at the (3,-1) BCPs of the H-bonds:

$$E_{C/O/NH\cdots O/N/O\cdots O/N} = 0.5 \cdot V(r), \quad (5)$$

where V(r) – value of a local potential energy at the (3,-1) BCP.

The energies of all others conventional AH···B H-bonds were evaluated by the empirical Iogansen's formula[45]:

$$E_{AH\cdots B} = 0.33 \cdot \sqrt{\Delta\nu - 40}, \quad (6)$$

where Δν – magnitude of the frequency shift of the stretching mode of the AH H-bonded group involved in the AH···B H-bond relatively the unbound group. The partial deuteration was applied to minimize the effect of vibrational resonances[46-48].

The energies of the N6H···N3 and N1H···O2 H-bonds in the $TS_{A+\cdot T\text{-}(w)\leftrightarrow A\cdot T^{*}O2\uparrow(w)}$ and $TS_{A+\cdot T\text{-}(w)\leftrightarrow A^{*}\cdot T\uparrow(w)}$, O6H···N3, N4H···N1 and N1H···N4 H-bonds in the $TS_{G\cdot C^{*}\uparrow(w)\leftrightarrow G^{*}\cdot C^{*}O2\uparrow(w)}$, $TS_{G\cdot C^{*}\downarrow(w)\leftrightarrow G^{*}NH3\cdot C\downarrow(w)}$ and $TS_{G^{*}\cdot C\downarrow(w)\leftrightarrow G^{*}N1\cdot C^{*}\downarrow(w)}$, respectively, containing loosened covalent bridges were estimated by the Nikolaienko-Bulavin-Hovorun formulas[49]:

$$E_{O6H\cdots N3} = 1.72 + 142 \cdot \rho, \quad (7)$$

$$E_{N6/N1/N4H\cdots N3/O2/N1/N4} = -2.03 + 225 \cdot \rho, \quad (8)$$

where ρ – the electron density at the (3,-1) BCP of the H-bond.

The atomic numbering scheme for the DNA bases is conventional[50].

Substantiation of the computational model. Similarly to our recent studies on the related topic[51,52], we have considered the simplest physico-chemical model of the base mispairs in the base-pair recognition pocket of the high-fidelity DNA-polymerase, namely the H-bonded pairs of nucleotide bases in the continuum with ε=1/ε=4. In this case, we have relied on the results obtained in the work[53], in which the adequacy of this model was convincingly proved, at least at the study of the tautomerisation of the H-bonded pairs of nucleotide bases, where insignificance of the influence of the stacking and the sugar-phosphate backbone on the tautomerisation process has been demonstrated. Thereby, their impact can be neglected in the first approximation. In addition, the applied model can help to distinguish the lowest structural level, at which the tautomerisation effects can be observed, and to estimate the changes at the sequential complication of the model.

In this study we have chosen the simplest level of the base pairs that adequately reflects the processes occurring in real systems[54] without deprivation of the structurally functional properties of the bases in the composition of DNA. In this case, the value of the effective dielectric constant ε ($1 < \varepsilon < 4$), that is characteristic for the anhydrous molecular crystals, satisfactorily models the substantially hydrophobic recognition pocket of the DNA-polymerase machinery as a part of the replisome[55-57].

2. Numerical and Graphical Materials.

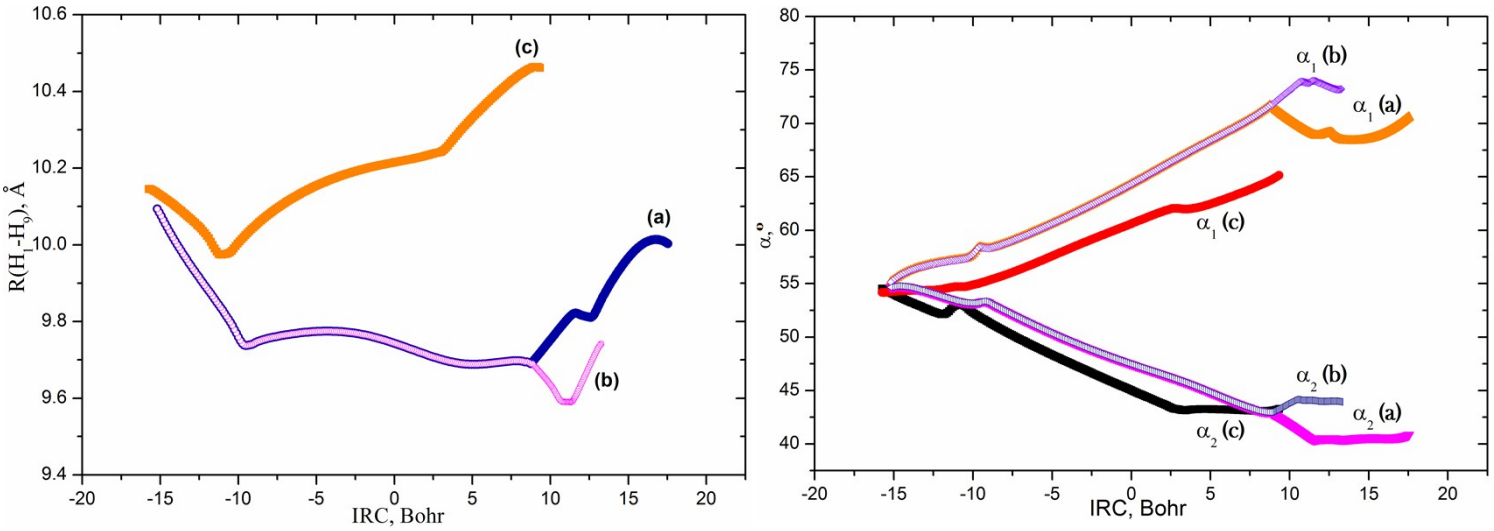

Figure S1. Profiles of the $R(H_1\text{-}H_9)$ distances between the H_1 and H_9 glycosidic hydrogens and the α_1 ($\angle N1H_1(T)H_9(A)$) or α_2 ($\angle N9H_9(A)H_1(T)$) glycosidic angles of the T and A bases, respectively, along the IRC of the (**a**) A·T(WC)↔A*·T$_{\uparrow}$(w); (**b**) A·T(WC)↔A·T*$_{O2\uparrow}$(w) and (**c**) A·T(WC)↔A·T*$_{\downarrow}$(w) tautomerisations *via* the sequential DPT accompanied with structural rearrangement (B3LYP/6-311++G(d,p) level of theory (ε=1)) (see also Figs. 1, 2). Continuity of the depicted dependencies and range of their changes unequivocally indicates the non-dissociative nature of the tautomerisation processes.

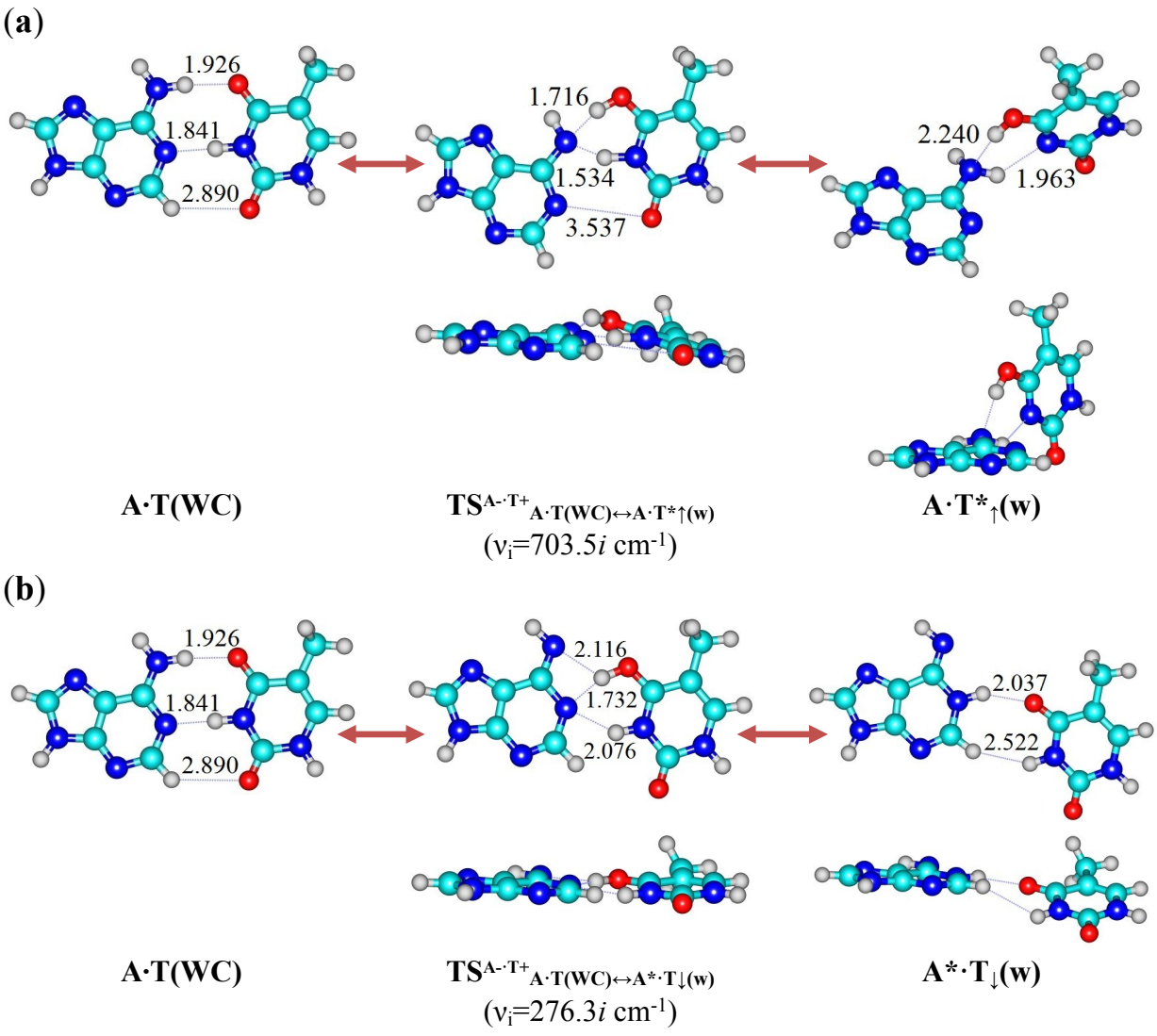

Figure S2. Mutagenic tautomeric variability of the A·T(WC) DNA base pair: high-energy reaction pathways of the tautomeric transformations of the A·T(WC) DNA base pair *via* the sequential DPT accompanied with structural rearrangements to wobble mismatches (B3LYP/6-311++G(d,p) level of theory (ε=1)). Depicted structures correspond to the stationary points on the reaction pathways of the (**a**) A·T(WC)↔A·T*$_{\uparrow}$(w) and (**b**) A·T(WC)↔A*·T$_{\downarrow}$(w) tautomeric conversions (see also Fig. 4 and S5 and Tables S1-S4). Perpendicular projections of all complexes are given below them. Dotted lines indicate AH···B H-bonds or O···N van der Waals contact (their lengths in the continuum with ε=1 are presented in angstroms; their basic physico-chemical characteristics – electron-topological, structural, vibrational and energetic characteristics are presented in Table S1); carbon atoms are in light-blue, nitrogen – in dark-blue, hydrogen – in grey and oxygen – in red; ν_i – imaginary frequency. The TS$^{A-\cdot T+}_{A\cdot T(WC)\leftrightarrow A\cdot T^*\uparrow(w)}$, A·T*$_{\uparrow}$(w) and A*·T$_{\downarrow}$(w) H-bonded complexes possess non-planar structures and are characterized by the following values of the ∠C6N1(A$^-$)C2N3(C$^+$)=10.6º, ∠C6N1(A)N3C4(C)=87.6º and ∠N1C2(A)N3C4(C)=17.6º dihedral angles, respectively. The A·T*$_{\uparrow}$(w) and A*·T$_{\downarrow}$(w) mismatches are thermodynamically unstable structures with $\Delta G_{int}>0$ (see Table S3) and can be really registered only under the condition of their stabilization by the stacking interactions with neighboring Watson-Crick DNA base pairs.

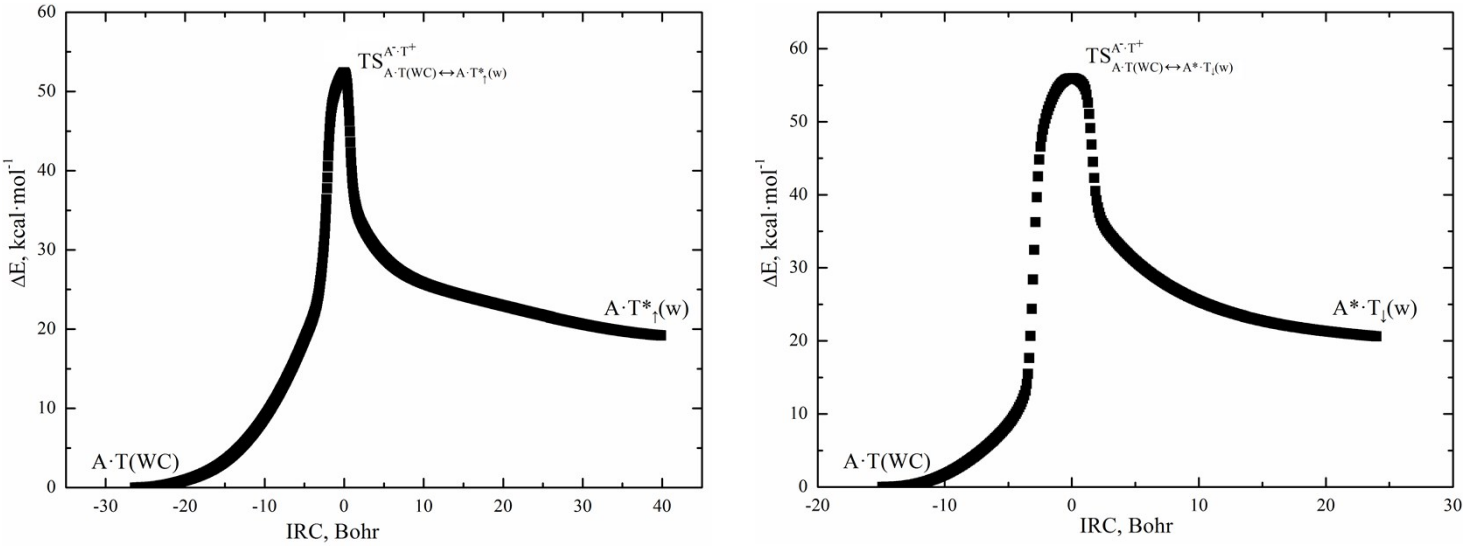

Figure S3. Profiles of the relative electronic energy ΔE of the DNA base pairs along the IRC of the (**a**) A·T(WC)↔A·T*$_{\uparrow}$(w) and (**b**) A·T(WC)↔A*·T$_{\downarrow}$(w) tautomerisations *via* the sequential DPT accompanied with structural rearrangements of the bases relative to each other. Presented data are obtained by following IRC at the B3LYP/6-311++G(d,p) level of theory in the continuum with ε=1.

Table S1. Electron-topological, structural, vibrational and energetic characteristics of the intermolecular H-bonds in the investigated DNA base pairs and TSs of their tautomerisation *via* the sequential DPT accompanied with structural rearrangements of the bases relative to each other, their energetic and polar characteristics obtained at the B3LYP/6-311++G(d,p) level of theory (ε=1).

Base pair/TS	AH···B H-bond/ O···N van der Waals contact	ρ[a]	$\Delta\rho$[b]	$100\cdot\varepsilon$[c]	$d_{A\cdots B}$/ $d_{O\cdots N}$[d]	$d_{H\cdots B}$/ $d_{H\cdots H}$[e]	Δd_{AH}[f]	∠AH···B[g]	$\Delta\nu$[h]	$E_{AH\cdots B}$/ $E_{O\cdots N}$[i]	ΔG[j]	μ[k]
	N6H···O4	0.026	0.093	4.39	2.946	1.926	0.014	173.5	238.7	4.65	0.00	1.88
A·T(WC)[56]	N3H···N1	0.040	0.093	6.49	2.886	1.841	0.032	178.8	567.5	7.58		
	C2H···O2	0.004	0.014	3.40	3.975	2.890	0.0002	132.3	-4.8	0.74*		
A*·T$_{\uparrow}$(w)	N3H···N6	0.042	0.095	6.21	2.858	1.806	0.039	173.3	674.2	8.31	9.90	4.29
	N1H···O6	0.034	0.115	4.40	2.845	1.814	0.018	177.0	316.7	5.49		
TS$_{A+\cdot T-(w)\leftrightarrow A\cdot T^{*}O2\uparrow(w)}$	N6H···N3	0.047	0.099	6.37	2.800	1.765	-	168.0	-	8.57**	10.73	5.63
A·T*$_{O2\uparrow}$(w)	N6H···N3	0.034	0.088	1.71	2.944	1.915	0.020	167.1	391.9	6.19	10.91	3.96
	O2H···N1	0.071	0.081	0.86	2.644	1.608	0.067	171.9	1239.6	11.43		
TS$_{A+\cdot T-(w)\leftrightarrow A^{*}\cdot T\uparrow(w)}$	N1H···O2	0.058	0.141	4.11	2.677	1.616	-	179.2	-	10.91**	11.67	5.32
A^{+}·T^{-}(w)	N6^{+}H···N3^{-}	0.069	0.086	5.82	2.693	1.609	0.078	173.8	1314.2	11.78	12.43	6.86
	N1^{+}H···O2^{-}	0.076	0.140	3.66	2.602	1.508	0.080	180.0	1261.5	11.53		
A·T*$_{\downarrow}$(w)	O4H···N1	0.055	0.100	5.18	2.707	1.693	0.044	171.4	855.6	9.42	13.08	4.57
	C2H···N3	0.009	0.026	0.79	3.699	2.614	-	129.0	-19.5	1.41*		
TS$^{A+\cdot T-}_{A\cdot T(WC)\leftrightarrow A+\cdot T-(w)}$	N6^{+}H···O4^{-}	0.020	0.065	16.30	3.102	2.070	0.024	153.2	377.5	2.82	16.72	6.77
	N6^{+}H···N3^{-}	0.023	0.075	0.89	3.097	2.064	0.024	140.7	377.5	3.24		
	N1^{+}H···N3^{-}	0.022	0.075	53.95	3.136	2.090	0.032	139.6	503.7	2.55		
	N1^{+}H···O2^{-}	0.034	0.101	4.19	2.893	1.847	0.032	150.4	503.7	4.56		
A·T*$_{\uparrow}$(w)	N6H···N3	0.017	0.056	10.90	3.018	2.240	0.013	132.0	194.5	4.10	17.47	4.16
	O4H···N6	0.028	0.078	6.20	2.930	1.963	0.016	166.1	322.7	5.55		
TS$^{A+\cdot T-}_{A\cdot T(WC)\leftrightarrow A\cdot T^{*}\downarrow(w)}$	N6^{+}H···O4^{-}	0.023	0.097	6.47	2.974	1.953	0.012	140.6	188.0	4.01	20.28	7.77
	N1^{+}H···O4^{-}	0.055	0.128	0.19	2.723	1.656	0.053	153.6	1668.9	13.32		
	C2^{+}H···N3^{-}	0.009	0.030	57.50	3.751	2.665	0.002	113.5	-28.1	1.60*		
A*·T$_{\downarrow}$(w)	N1H···O4	0.018	0.075	3.14	2.982	2.037	0.006	153.3	87.8	2.28	23.12	5.89
	N3H···HC2	0.003	0.010	32.79	3.291	2.522	-	132.5	-3.1	0.46*		
TS$^{A-\cdot T+}_{A\cdot T(WC)\leftrightarrow A\cdot T^{*}\uparrow(w)}$	O4^{+}H···N6^{-}	0.049	0.108	5.82	2.654	1.716	0.042	152.5	783.7	9.00	48.89	9.55
	N3^{+}H···N6^{-}	0.084	0.050	5.58	2.625	1.534	0.130	156.3	1499.3	12.61		
	O2^{+}···N1^{-}	0.004	0.012	18.39	3.537	-	-	-	-	0.67*		
TS$^{A-\cdot T+}_{A\cdot T(WC)\leftrightarrow A^{*}\cdot T\downarrow(w)}$	O4^{+}H···N6^{-}	0.020	0.072	328.10	2.847	2.116	0.077	124.9	1188.6	2.72	53.03	11.83
	O4^{+}H···N1^{-}	0.050	0.078	0.78	2.747	1.732	0.077	162.2	1188.6	8.46		
	N3^{+}H···N1^{-}	0.023	0.073	8.90	2.960	2.076	0.008	143.1	138.4	3.27		
2AP·T(WC)	C6H···O4	0.005	0.016	2.18	3.879	2.792	0.0004	132.0	-3.1	0.90*	0.00	3.15
	N3H···N1	0.040	0.095	6.42	2.876	1.832	0.032	179.3	567.1	7.58		
	N2H···O2	0.023	0.082	5.68	2.998	1.982	0.010	174.9	171.4	3.78		
2AP·T*$_{\downarrow}$(w)	O4H···N1	0.057	0.097	5.05	2.698	1.678	0.050	169.2	954.1	9.98	7.33	1.52
	N2H···N3	0.029	0.085	7.39	2.987	1.965	0.016	168.9	295.0	5.27		
TS$^{2AP+\cdot T-}_{2AP\cdot T(WC)\leftrightarrow 2AP\cdot T^{*}\downarrow(w)}$	N1^{+}H···O4^{-}	0.033	0.099	7.55	2.918	1.869	0.036	143.2	567.7	4.48	15.48	6.45
	N1^{+}H···N3^{-}	0.025	0.081	26.93	3.064	2.015	0.036	146.1	567.7	3.10		
	N2^{+}H···N3^{-}	0.022	0.070	3.88	3.119	2.093	0.013	143.7	296.8	3.09		
	N2^{+}H···O2^{-}	0.016	0.053	34.47	3.201	2.175	0.019	151.8	296.8	2.20		

[a]The electron density at the (3,-1) BCP of the H-bond, a.u.; [b]The Laplacian of the electron density at the (3,-1) BCP of the H-bond, a.u.; [c]The ellipticity at the (3,-1) BCP of the H-bond; [d]The distance between the A (H-bond donor) and B (H-bond acceptor) atoms of the AH···B H-bond, Å; [e]The distance between the H and B atoms of the AH···B H-bond, Å; [f]The elongation of the H-bond donating group AH upon the AH···B H-bonding, Å; [g]The H-bond angle, degree; [h]The redshift of the stretching vibrational mode ν(AH) of the AH H-bonded group, cm^{-1}; [i]Energy of the H-bonds, calculated by Iogansen's[45], Espinose-Molins-Lecomte (EML)[42-44] (marked with an asterisk) or Nikolaienko-Bulavin-Hovorun (marked with double asterisk)[49] formulas and energy of the attractive O···N van der Waals contact calculated by EML formula[42-44], kcal·mol^{-1}; [j]The relative Gibbs free energy of the complex obtained at the MP2/aug-cc-pVDZ//B3LYP/6-311++G(d,p) level of theory under normal conditions, kcal·mol^{-1}; [k]The dipole moment of the complex, D.

Table S2. Energetic characteristics of the investigated DNA base pairs and TSs of their tautomerisation *via* the sequential DPT accompanied with structural rearrangements of the bases relative to each other obtained at the different levels of theory for the geometry calculated at the B3LYP/6-311++G(d,p) level of theory in the continuum with ε=1/ε=4.

Complex	MP2/6-311++G(2df,pd)				MP2/cc-pVQZ				MP2/aug-cc-pVDZ			
	ε=1		**ε=4**		**ε=1**		**ε=4**		**ε=1**		**ε=4**	
	ΔG^a	ΔE^b	ΔG^a	ΔE^b	ΔG^a	ΔE^b	ΔG^a	ΔE^b	ΔG^a	ΔE^b	ΔG^a	ΔE^b
A·T(WC)	0.00	0.00	0.00	0.00	0.00	0.00	0.00	0.00	0.00	0.00	0.00	0.00
A*·T$_{\uparrow}$(w)	9.97	9.66	9.43	8.88	9.89	9.58	9.39	8.84	9.90	9.59	9.32	8.78
TS$_{A+\cdot T-(w)\leftrightarrow A\cdot T*O2\uparrow(w)}$	10.42	12.70	9.23	11.29	10.57	10.91	9.59	11.65	10.73	13.02	9.66	11.72
A·T*$_{O2\uparrow}$(w)	10.41	10.75	9.70	9.99	10.75	13.04	9.90	10.19	10.91	11.25	10.19	10.48
TS$_{A+\cdot T-(w)\leftrightarrow A*\cdot T\uparrow(w)}$	11.75	13.91	10.95	12.82	12.02	14.18	11.24	13.11	11.67	13.83	10.84	12.72
A$^+$·T$^-$(w)	12.52	13.44	10.57	10.91	12.76	14.51	10.81	11.15	12.43	13.36	10.39	10.73
A·T*$_{\downarrow}$(w)	12.47	14.23	10.52	11.79	12.79	13.71	10.87	12.14	13.08	14.84	11.20	12.47
TS$^{A+\cdot T-}_{A\cdot T(WC)\leftrightarrow A+\cdot T-(w)}$	17.44	16.74	15.08	14.23	16.77	17.64	14.87	14.02	16.72	16.02	14.41	13.56
A·T*$_{\uparrow}$(w)	16.53	17.40	-	-	17.13	16.42	-	-	17.47	18.34	-	-
TS$^{A+\cdot T-}_{A\cdot T(WC)\leftrightarrow A\cdot T*\downarrow(w)}$	20.82	20.95	16.48	16.86	20.67	20.80	16.35	16.73	20.28	20.41	16.03	16.42
A*·T$_{\downarrow}$(w)	22.50	22.01	-	-	22.51	22.01	-	-	23.12	22.62	-	-
TS$^{A-\cdot T+}_{A\cdot T(WC)\leftrightarrow A\cdot T*\uparrow(w)}$	48.26	49.33	-	-	48.64	49.72	-	-	48.89	49.96	-	-
TS$^{A-\cdot T+}_{A\cdot T(WC)\leftrightarrow A*\cdot T\downarrow(w)}$	53.30	53.04	-	-	53.41	53.15	-	-	53.03	52.77	-	-
2AP·T(WC)	0.00	0.00	0.00	0.00	0.00	0.00	0.00	0.00	0.00	0.00	0.00	0.00
2AP·T*$_{\downarrow}$(w)	8.17	7.88	6.93	7.39	8.37	8.08	7.17	7.63	8.62	8.33	7.33	7.79
TS$^{2AP+\cdot T-}_{2AP\cdot T(WC)\leftrightarrow 2AP\cdot T*\downarrow(w)}$	19.30	18.17	16.16	15.41	19.01	17.88	15.95	15.19	18.66	17.53	15.48	14.72

[a]The relative Gibbs free energy of the investigated complexes (T=298.15 K), kcal·mol^{-1}; [b]The relative electronic energy of the investigated complexes, kcal·mol^{-1}.

Table S3. Interbase interaction energies (in kcal·mol^{-1}) for the investigated DNA base pairs and TSs of their conversions *via* the sequential DPT accompanied with structural rearrangements of the bases relative to each other obtained at the MP2/6-311++G(3df,2pd)//B3LYP/6-311++G(d,p) level of theory (ε=1).

Complex	$-\Delta E_{int}$[a]	ΣE_{HB}[b]	$\Sigma E_{HB}/\lvert\Delta E_{int}\rvert$, %	$-\Delta G_{int}$[c]
A·T(WC)	14.92	12.97	86.9	1.43
A*·T$_{\uparrow}$(w)	18.10	13.80	76.3	6.06
A·T*$_{O2\uparrow}$(w)	24.75	17.62	71.2	11.20
A^{+}·T^{-}(w)	131.37	23.31	17.7	119.92
A·T*$_{\downarrow}$(w)	13.44	10.83	80.6	1.61
TS$^{A+\cdot T-}_{A\cdot T(WC)\leftrightarrow A+\cdot T-(w)}$	123.44	13.17	10.7	110.37
A·T*$_{\uparrow}$(w)	9.17	9.65	105.2	-3.47
TS$^{A+\cdot T-}_{A\cdot T(w)\leftrightarrow A\cdot T^{*}\downarrow(w)}$	121.09	18.83	15.6	108.85
A*·T$_{\downarrow}$(w)	5.18	2.74	52.9	-7.01
TS$^{A-\cdot T+}_{A\cdot T(WC)\leftrightarrow A\cdot T^{*}\uparrow(w)}$	134.61	22.28	16.6	122.76
TS$^{A-\cdot T+}_{A\cdot T(WC)\leftrightarrow A^{*}\cdot T\downarrow(w)}$	119.16	14.45	12.1	105.98
2AP·T(WC)	14.28	12.26	85.9	2.88
2AP·T*$_{\downarrow}$(w)	20.95	15.25	72.8	9.18
TS$^{2AP+\cdot T-}_{2AP\cdot T(WC)\leftrightarrow 2AP\cdot T^{*}\downarrow(w)}$	122.78	12.87	10.5	108.58

[a]The BSSE-corrected electronic interaction energy; [b]The total energy of the intermolecular H-bonds (see Table S1); [c]The BSSE-corrected Gibbs free energy of interaction (T=298.15 K).

Table S4. Energetic and kinetic characteristics of the (**a**) A·T(WC)↔A^+·T^-(w), (**b**) A^+·T^-(w)↔A*·$T_\uparrow$(w), (**c**) A^+·T^-↔A·T*$_{O2\uparrow}$(w), (**d**) A·T(WC)↔A·T*$_\downarrow$(w), (**e**) A·T(WC)↔A·T*$_\uparrow$(w), (**f**) A·T(WC)↔A*·$T_\downarrow$(w) and (**g**) 2AP·T(WC)↔2AP·T*$_\downarrow$(w) tautomerisations *via* the sequential DPT accompanied with structural rearrangements of the bases relative to each other obtained at the different levels of theory for the geometry calculated at the B3LYP/6-311++G(d,p) level of theory in the continuum with ε=1/ε=4.

Level of theory	ΔG^a	ΔE^b	$\Delta\Delta G_{TS}^c$	$\Delta\Delta E_{TS}^d$	$\Delta\Delta G^e$	$\Delta\Delta E^f$	$\tau_{99.9\%}^g$
(a) A·T(WC)↔A^+·T^-(w)							
ε=1 (ν_i=128.5*i* cm^{-1})							
MP2/6-311++G(2df,pd)	12.52	13.44	17.44	16.74	4.92	3.30	$4.48\cdot10^{-9}$
MP2/cc-pVQZ	12.79	13.71	17.13	16.42	4.34	2.71	$1.68\cdot10^{-9}$
MP2/aug-cc-pVDZ	12.43	13.36	16.72	16.02	4.29	2.66	$1.54\cdot10^{-9}$
ε=4 (ν_i=113.8*i* cm^{-1})							
MP2/6-311++G(2df,pd)	10.57	10.91	15.08	14.23	4.51	3.32	$2.24\cdot10^{-9}$
MP2/cc-pVQZ	10.81	11.15	14.87	14.02	4.07	2.87	$1.06\cdot10^{-9}$
MP2/aug-cc-pVDZ	10.39	10.73	14.41	13.56	4.03	2.83	$9.86\cdot10^{-10}$
(b) A^+·T^-(w)↔A*·$T_\uparrow$(w)							
ε=1 (ν_i=835.7*i* cm^{-1})							
MP2/6-311++G(2df,pd)	-2.55	-3.78	-0.76	0.47	1.78	4.26	$1.86\cdot10^{-13}$
MP2/cc-pVQZ	-2.89	-4.13	-0.76	0.47	2.13	4.60	$1.87\cdot10^{-13}$
MP2/aug-cc-pVDZ	-2.53	-3.77	-0.76	0.47	1.77	4.24	$1.85\cdot10^{-13}$
ε=4 (ν_i=1097.1*i* cm^{-1})							
MP2/6-311++G(2df,pd)	-1.14	-2.03	0.38	1.91	1.52	3.94	$8.84\cdot10^{-13}$
MP2/cc-pVQZ	-1.42	-2.30	0.43	1.97	1.85	4.27	$1.01\cdot10^{-12}$
MP2/aug-cc-pVDZ	-1.06	-1.95	0.45	1.99	1.52	3.94	$9.86\cdot10^{-13}$
(c) A^+·T^-(w)↔A·T*$_{O2\uparrow}$(w)							
ε=1 (ν_i=700.3*i* cm^{-1})							
MP2/6-311++G(2df,pd)	-2.11	-2.69	-2.10	-0.74	0.01	1.96	$2.16\cdot10^{-14}$
MP2/cc-pVQZ	-2.22	-2.80	-2.04	-0.67	0.18	2.13	$2.42\cdot10^{-14}$
MP2/aug-cc-pVDZ	-1.52	-2.11	-1.71	-0.34	-0.18	1.77	$4.02\cdot10^{-14}$
ε=4 (ν_i=869.2*i* cm^{-1})							
MP2/6-311++G(2df,pd)	-0.87	-0.92	-1.34	0.38	-0.47	1.30	$5.63\cdot10^{-14}$
MP2/cc-pVQZ	-0.90	-0.95	-1.21	0.50	-0.31	1.46	$7.02\cdot10^{-14}$
MP2/aug-cc-pVDZ	-0.19	-0.24	-0.73	0.99	-0.54	1.23	$1.12\cdot10^{-13}$
(d) A·T(WC)↔A·T*$_\downarrow$(w)							
ε=1 (ν_i=99.7*i* cm^{-1})							
MP2/6-311++G(2df,pd)	12.47	14.23	20.82	20.95	8.35	6.73	$1.47\cdot10^{-6}$
MP2/cc-pVQZ	12.76	14.51	20.67	20.80	7.91	6.28	$6.97\cdot10^{-7}$
MP2/aug-cc-pVDZ	13.08	14.84	20.28	20.41	7.20	5.57	$2.09\cdot10^{-7}$
ε=4 (ν_i=79.4*i* cm^{-1})							
MP2/6-311++G(2df,pd)	10.01	11.79	16.48	16.86	6.47	5.07	$6.13\cdot10^{-8}$
MP2/cc-pVQZ	10.36	12.14	16.35	16.73	5.99	4.59	$2.75\cdot10^{-8}$
MP2/aug-cc-pVDZ	10.69	12.47	16.03	16.42	5.34	3.94	$9.20\cdot10^{-9}$
(e) A·T(WC)↔A·T*$_\uparrow$(w)							
ε=1 (ν_i=703.5*i* cm^{-1})							
MP2/6-311++G(2df,pd)	16.53	17.40	48.26	49.33	31.73	31.93	$1.44\cdot10^{11}$
MP2/cc-pVQZ	16.77	17.64	48.64	49.72	31.87	32.08	$1.84\cdot10^{11}$
MP2/aug-cc-pVDZ	17.47	18.34	48.89	49.96	31.42	31.63	$6.62\cdot10^{10}$
(f) A·T(WC)↔A*·$T_\downarrow$(w)							
ε=1 (ν_i=276.3*i* cm^{-1})							
MP2/6-311++G(2df,pd)	22.50	22.01	53.30	53.04	30.80	31.04	$4.05\cdot10^{10}$
MP2/cc-pVQZ	22.51	22.01	53.41	53.15	30.90	31.14	$4.81\cdot10^{10}$
MP2/aug-cc-pVDZ	23.12	22.62	53.03	52.77	29.91	30.15	$9.06\cdot10^{9}$
(g) 2AP·T(WC)↔2AP·T*$_\downarrow$(w)							
ε=1 (ν_i=112.3*i* cm^{-1})							
MP2/6-311++G(2df,pd)	8.17	7.88	19.30	18.17	11.13	10.29	$1.59\cdot10^{-4}$
MP2/cc-pVQZ	8.37	8.08	19.01	17.88	10.64	9.81	$6.98\cdot10^{-5}$
MP2/aug-cc-pVDZ	8.62	8.33	18.66	17.53	10.04	9.21	$2.53\cdot10^{-5}$
ε=4							
MP2/6-311++G(2df,pd)	6.93	7.39	16.16	15.41	9.23	8.01	$6.48\cdot10^{-6}$
MP2/cc-pVQZ	7.17	7.63	15.95	15.19	8.78	7.56	$3.01\cdot10^{-6}$
MP2/aug-cc-pVDZ	7.33	7.79	15.48	14.72	8.15	6.93	$1.04\cdot10^{-6}$

[a]The Gibbs free energy of the product relatively the reactant of the tautomerisation reaction (T=298.15 K), kcal·mol^{-1}; [b]The electronic energy of the product relatively the reactant of the tautomerisation reaction, kcal·mol^{-1}; [c]The Gibbs free energy barrier for the forward reaction of tautomerisation, kcal·mol^{-1}; [d]The electronic energy barrier for the forward reaction of tautomerisation, kcal·mol^{-1}; [e]The Gibbs free energy barrier for the reverse reaction of tautomerisation, kcal·mol^{-1}; [f]The electronic energy barrier for the reverse reaction of tautomerisation, kcal·mol^{-1}; [g]The time necessary to reach 99.9% of the equilibrium concentration between the reactant and the product of the tautomerisation reaction, s; See also summary Table S2 for the Gibbs and electronic energies of the mispairs and TSs relatively the global minimum – the A·T(WC) DNA base pair.

Table S5. Patterns of the specific intermolecular interactions including AH···B H-bonds and loosened A-H-B covalent bridges that sequentially replace each other along the IRC of the biologically important A·T(WC)↔A*·$T_{\uparrow}$(w), A·T(WC)↔A·T*$_{O2\uparrow}$(w) and A·T(WC)↔A·T*$_{\downarrow}$(w) tautomerisations *via* the sequential DPT accompanied with structural rearrangements of the bases relative to each other and their ranges of the existence obtained at the B3LYP/6-311++G(d,p) level of theory at ε=1 (see also Figs. 1, 2 and 3).

Patterns	IRC ranges, Bohr	Intermolecular interactions, forming patterns
A·T(WC)↔A*·$T_{\uparrow}$(w)		
I	[-15.19÷-9.38)	(A)N6H···O4(T), (T)N3H···N1(A), (A)C2H···O2(T)
II	[-9.38÷-8.88)	(A)N6H···O4(T), (T)N3-H-N1(A), (A)C2H···O2(T)
III	[-8.88÷-3.17)	(A)N6H···O4(T), (A)N1H···N3(T), (A)C2H···O2(T)
IV	[-3.17÷-2.92)	(A)N6H···O4(T), (A)N1H···N3(T), (A)N1H···O2(T), (A)C2H···O2(T)
V	[-2.92÷0.76)	(A)N6H···O4(T), (A)N6H···N3(T), (A)N1H···N3(T), (A)N1H···O2(T)
VI	[0.76÷1.65)	(A)N6H···O4(T), (A)N6H···N3(T), (A)N1H···O2(T)
VII	[1.65÷11.99]	(A)N6H···N3(T), (A)N1H···O2(T)
VIII	[11.99÷12.41)	(A)N6-H-N3(T), (A)N1H···O2(T)
IX	[12.41÷17.54]	(T)N3H···N6(A), (A)N1H···O2(T)
A·T(WC)↔A·T*$_{O2\uparrow}$(w)		
I	[-15.19÷-9.38)	(A)N6H···O4(T), (T)N3H···N1(A), (A)C2H···O2(T)
II	[-9.38÷-8.88)	(A)N6H···O4(T), (T)N3-H-N1(A), (A)C2H···O2(T)
III	[-8.88÷-3.17)	(A)N6H···O4(T), (A)N1H···N3(T), (A)C2H···O2(T)
IV	[-3.17÷-2.92)	(A)N6H···O4(T), (A)N1H···N3(T), (A)N1H···O2(T), (A)C2H···O2(T)
V	[-2.92÷0.76)	(A)N6H···O4(T), (A)N6H···N3(T), (A)N1H···N3(T), (A)N1H···O2(T)
VI	[0.76÷1.65)	(A)N6H···O4(T), (A)N6H···N3(T), (A)N1H···O2(T)
VII	[1.65÷10.82)	(A)N6H···N3(T), (A)N1H···O2(T)
VIII	[10.82÷11.24)	(A)N6H···N3(T), (A)N1-H-O2(T)
IX	[11.24÷13.26]	(A)N6H···N3(T), (T)O2H···N1(A)
A·T(WC)↔A·T*$_{\downarrow}$(w)		
I	[-15.74÷-10.78)	(A)N6H···O4(T), (T)N3H···N1(A), (A)C2H···O2(T)
II	[-10.78÷-10.29)	(A)N6H···O4(T), (T)N3-H-N1(A), (A)C2H···O2(T)
III	[-10.29÷-6.15)	(A)N6H···O4(T), (A)N1H···N3(T), (A)C2H···O2(T)
IV	[-6.15÷-4.27)	(A)N6H···O4(T), (A)N1H···N3(T)
V	[-4.27÷-0.88)	(A)N6H···O4(T), (A)N1H···O4(T), (A)N1H···N3(T)
VI	[-0.88÷-0.50)	(A)N6H···O4(T), (A)N1H···O4(T), (A)N1H···N3(T), (A)C2H···N3(T)
VII	[-0.50÷2.51)	(A)N6H···O4(T), (A)N1H···O4(T), (A)C2H···N3(T)
VIII	[2.51÷3.00)	(A)N6H···O4(T), (A)N1-H-O4(T), (A)C2H···N3(T)
IX	[3.00÷5.70)	(A)N6H···O4(T), (T)O4H···N1(T), (A)C2H···N3(T)
X	[5.70÷9.34]	(T)O4H···N1(T), (A)C2H···N3(T)

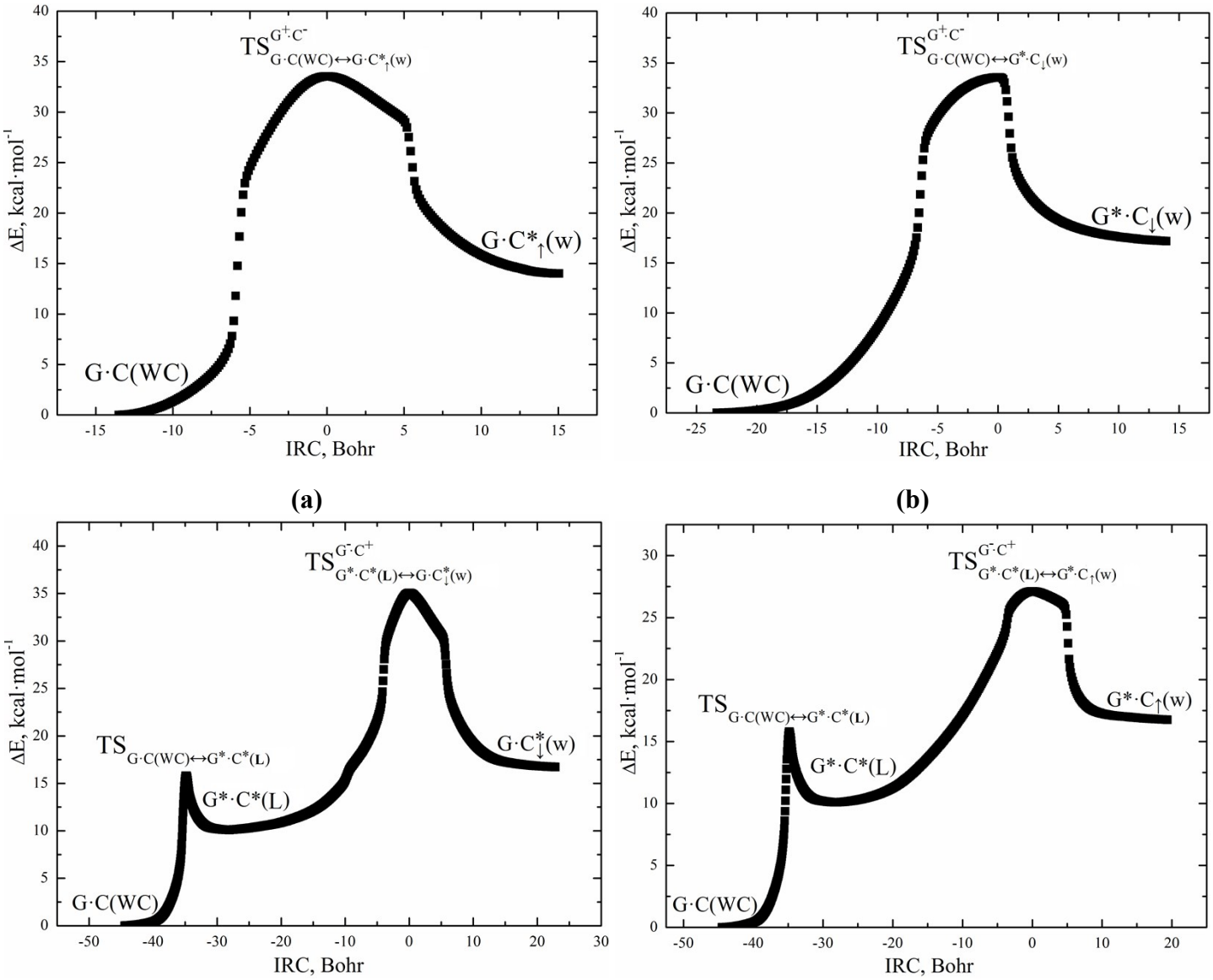

Figure S4. Profiles of the relative electronic energy ΔE of the DNA base pairs along the IRC of the (**a**) G·C(WC)↔G·C*↑(w), (**b**) G·C(WC)↔G*·C↓(w), (**c**) G·C(WC)↔G*·C*(L)↔G·C*↓(w) and (**d**) G·C(WC)↔G*·C*(L)↔G*·C↑(w) tautomerisations *via* the sequential DPT accompanied with structural rearrangements of the bases relative to each other. Presented data are obtained by following IRC at the B3LYP/6-311++G(d,p) level of theory in the continuum with ε=1.

Table S6. Electron-topological, structural, vibrational and energetic characteristics of the intermolecular H-bonds in the investigated DNA base pairs and TSs of their tautomerisation *via* the sequential DPT accompanied with structural rearrangements of the bases relative to each other, their energetic and polar characteristics obtained at the B3LYP/6-311++G(d,p) level of theory (ε=1).

Base pair/TS	AH···B H-bond	ρ^a	$\Delta\rho^b$	$100\cdot\varepsilon^c$	$d_{A\cdots B}{}^d$	$d_{H\cdots B}{}^e$	$\Delta d_{AH}{}^f$	∠AH···B^g	$\Delta\nu^h$	$E_{AH\cdots B}{}^i$	ΔG^j	μ^k
G·C(WC)[57]	N4H···O6	0.037	0.120	3.71	2.809	1.774	0.027	178.8	457.4	6.78	0.00	6.04
	N1H···N3	0.033	0.088	6.93	2.954	1.922	0.020	177.1	363.1	5.90		
	N2H···O2	0.027	0.094	5.77	2.936	1.915	0.012	178.4	213.7	5.11		
G*·C*(L)[57]	O6H···N4	0.051	0.103	5.27	2.720	1.714	0.038	172.1	745.6	8.72	8.74	6.09
	N3H···N1	0.038	0.089	6.36	2.910	1.865	0.034	176.7	595.4	7.74		
	N2H···O2	0.022	0.080	5.73	3.014	2.001	0.007	177.3	132.8	3.16		
TS$_{G\cdot C(WC)\leftrightarrow G^*\cdot C^*(L)}$[57]	N2H···O2	0.026	0.096	5.25	2.935	1.927	-	171.8	-	3.82*	10.35	7.66
G·C*$_{\uparrow}$(w)	N3H···O6	0.029	0.099	4.35	2.910	1.877	0.022	170.7	353.4	5.84	13.35	7.28
	N1H···O2	0.035	0.120	3.21	2.827	1.798	0.016	176.9	297.6	5.30		
G*·C$_{\uparrow}$(w)	N4H···O6	0.019	0.075	4.20	2.910	2.056	0.006	140.4	97.3	2.50	14.85	4.79
	O6H···N3	0.036	0.096	3.99	2.734	1.868	0.027	143.7	483.9	6.95		
G·C*$_{\downarrow}$(w)	N1H···N4	0.021	0.065	5.86	3.061	2.109	0.010	154.0	170.1	3.76	15.08	7.36
	N2H···N4	0.016	0.051	9.32	3.069	2.281	0.007	133.4	116.2	2.88		
	N3H···N2	0.014	0.044	10.53	3.207	2.298	0.007	147.9	124.7	3.04		
G*·C$_{\downarrow}$(w)	N4H···N1	0.025	0.071	6.72	3.071	2.047	0.016	176.4	287.3	5.19	15.10	4.70
	N2H···N3	0.026	0.078	7.93	3.032	2.011	0.015	170.2	267.8	4.98		
TS$_{G\cdot C^*\uparrow(w)\leftrightarrow G^*\cdot C^*O2\uparrow(w)}$	O6H···N3	0.068	0.088	4.84	2.644	1.606	-	179.4	-	11.39**	23.96	6.68
	N2H···O2	0.008	0.038	875.70	3.144	2.425	-	127.7	-	1.92*		
TS$^{G^{-}\cdot C^{+}}_{G^*\cdot C^*(L)\leftrightarrow G^*\cdot C\uparrow(w)}$	N4$^+$H···O6$^-$	0.079	0.165	5.33	2.565	1.479	0.075	155.0	1188.8	11.18	24.87	10.56
	N3$^+$H···O6$^-$	0.030	0.093	4.67	2.969	1.924	0.030	137.1	463.7	6.79		
G*·C*$_{O2\uparrow}$(w)	O6H···N3	0.051	0.097	5.12	2.729	1.717	0.044	179.2	838.6	9.33	25.26	6.67
	O2H···N1	0.081	0.078	4.80	2.594	1.542	0.084	173.0	1516.9	12.68		
TS$_{G\cdot C^*\downarrow(w)\leftrightarrow G^*NH3\cdot C\downarrow(w)}$	N4H···N1	0.059	0.096	6.30	2.725	1.668	-	169.2	-	11.34**	26.96	10.13
G*$_{NH3}$·C$_{\downarrow}$(w)	N4H···N1	0.039	0.096	6.70	2.865	1.839	0.031	168.7	534.5	7.34	27.16	8.54
	N2H···N3	0.064	0.089	5.14	2.733	1.644	0.067	177.4	1085.4	10.67		
TS$^{G^{+}\cdot C^{-}}_{G\cdot C(WC)\leftrightarrow G\cdot C^*\uparrow(w)}$	O6$^+$H···N4$^-$	0.017	0.056	52.36	3.178	2.174	0.038	137.9	638.3	2.69	30.47	6.05
	O6$^+$H···N3$^-$	0.029	0.074	1.38	2.968	1.963	0.038	155.7	638.3	5.39		
	N1$^+$H···N3$^-$	0.021	0.072	41.14	3.144	2.106	0.024	141.7	393.3	2.31		
	N1$^+$H···O2$^-$	0.031	0.096	5.40	2.935	1.897	0.024	149.3	393.3	3.89		
	N2$^+$H···O2$^-$	0.027	0.112	1.66	2.893	1.873	0.013	149.5	205.6	4.25		
TS$^{G^{-}\cdot C^{+}}_{G^*\cdot C^*(L)\leftrightarrow G\cdot C^*\downarrow(w)}$	N4$^+$H···O6$^-$	0.027	0.090	18.83	3.007	1.963	0.034	133.5	532.1	3.49	30.88	12.30
	N4$^+$H···N1$^-$	0.030	0.088	7.82	2.984	1.940	0.034	149.9	532.1	3.83		
	N3$^+$H···N1$^-$	0.015	0.047	17.21	3.325	2.291	0.019	137.5	294.8	2.52		
	N3$^+$H···N2$^-$	0.017	0.052	8.80	3.222	2.188	0.019	159.9	294.8	2.75		
TS$^{G^{+}\cdot C^{-}}_{G\cdot C(WC)\leftrightarrow G^*\cdot C\downarrow(w)}$	O6$^+$H···N4$^-$	0.025	0.072	15.36	3.021	2.035	0.019	151.6	361.8	5.92	31.08	2.71
	N1$^+$H···N4$^-$	0.080	0.072	6.16	2.664	1.551	0.099	164.7	1428.3	12.30		
	N2$^+$H···N3$^-$	0.036	0.090	6.94	2.922	1.884	0.032	163.7	529.2	7.30		
TS$_{G^*\cdot C\downarrow(w)\leftrightarrow G^*N1\cdot C^*\downarrow(w)}$	N1H···N4	0.059	0.093	6.15	2.752	1.678	-	178.4	-	11.17**	33.12	2.33
G*$_{N1}$·C*$_{\downarrow}$(w)	N1H···N4	0.040	0.094	6.42	2.878	1.834	0.032	177.2	572.8	7.62	34.58	2.32
	N3H···N2	0.052	0.096	6.49	2.786	1.719	0.055	178.9	926.8	9.83		

For the detailed designations see footnotes of the Table S1.

Table S7. Energetic characteristics of the investigated DNA base pairs and TSs of their tautomerisation *via* the sequential DPT accompanied with structural rearrangements of the bases relative to each other obtained at the MP2/6-311++G(2df,pd) and MP2/aug-cc-pVDZ levels of theory for the geometry calculated at the B3LYP/6-311++G(d,p) level of theory in the continuum with ε=1/ε=4.

Complex	MP2/6-311++G(2df,pd)				MP2/aug-cc-pVDZ			
	ε=1		**ε=4**		**ε=1**		**ε=4**	
	ΔG^a	ΔE^b	ΔG^a	ΔE^b	ΔG^a	ΔE^b	ΔG^a	ΔE^b
G·C(WC)	0.00	0.00	0.00	0.00	0.00	0.00	0.00	0.00
G*·C*(L)	8.24	7.89	9.44	8.84	8.74	8.39	9.98	9.39
$\mathbf{TS_{G\cdot C(WC)\leftrightarrow G^*\cdot C^*(L)}}$	9.73	13.06	8.93	9.96	10.35	13.68	9.21	10.24
$\mathbf{G\cdot C^*_{\uparrow}(w)}$	12.94	13.69	11.59	12.06	13.35	14.10	12.08	12.55
$\mathbf{G^*\cdot C_{\uparrow}(w)}$	13.29	15.66	11.10	13.05	14.85	17.22	12.64	14.59
$\mathbf{G\cdot C^*_{\downarrow}(w)}$	14.31	15.19	12.87	14.24	15.08	15.96	14.11	15.48
$\mathbf{G^*\cdot C_{\downarrow}(w)}$	14.31	15.70	13.28	14.54	15.10	16.49	14.14	15.40
$\mathbf{TS_{G\cdot C^*\uparrow(w)\leftrightarrow G^*\cdot C^*O2\uparrow(w)}}$	22.92	26.42	-	-	23.96	27.47	-	-
$\mathbf{TS^{G^-\cdot C^+}_{G^*\cdot C^*(L)\leftrightarrow G^*\cdot C\uparrow(w)}}$	24.33	25.09	18.75	18.52	24.87	25.64	19.30	19.06
$\mathbf{G^*\cdot C^*_{O2\uparrow}(w)}$	24.27	25.95	-	-	25.26	26.94	-	-
$\mathbf{TS_{G\cdot C^*\downarrow(w)\leftrightarrow G^*NH3\cdot C\downarrow(w)}}$	27.08	29.21	-	-	26.96	29.09	-	-
$\mathbf{G^*_{NH3}\cdot C_{\downarrow}(w)}$	27.49	27.66	-	-	27.16	27.33	-	-
$\mathbf{TS^{G^+\cdot C^-}_{G\cdot C(WC)\leftrightarrow G\cdot C^*\uparrow(w)}}$	30.65	30.92	31.55	31.93	30.47	30.74	31.35	31.73
$\mathbf{TS^{G^-\cdot C^+}_{G^*\cdot C^*(L)\leftrightarrow G\cdot C^*\downarrow(w)}}$	31.14	31.67	24.45	24.74	30.88	31.41	24.31	24.59
$\mathbf{TS^{G^+\cdot C^-}_{G\cdot C(WC)\leftrightarrow G^*\cdot C\downarrow(w)}}$	30.49	30.94	32.02	31.91	31.08	31.53	32.50	32.40
$\mathbf{TS_{G^*\cdot C\downarrow(w)\leftrightarrow G^*N1\cdot C^*\downarrow(w)}}$	33.02	37.12	-	-	33.12	37.22	-	-
$\mathbf{G^*_{N1}\cdot C^*_{\downarrow}(w)}$	34.54	36.14	-	-	34.58	36.17	-	-

For the detailed designations see footnotes of the Table S2.

Table S8. Energetic characteristics of the investigated DNA base pairs and TSs of their tautomerisation involving C nucleobase and its modified analogue P *via* the sequential DPT accompanied with structural rearrangements of the bases relative to each other obtained at the MP2/6-311++G(2df,pd) and MP2/aug-cc-pVDZ levels of theory for the geometry calculated at the B3LYP/6-311++G(d,p) level of theory in the continuum with ε=1/ε=4.

Complex	MP2/6-311++G(2df,pd)								MP2/aug-cc-pVDZ							
	ε=1				**ε=4**				**ε=1**				**ε=4**			
	X=C		**X=P**		**X=C**		**X=P**		**X=C**		**X=P**		**X=C**		**X=P**	
	ΔG	ΔE	ΔG	ΔE	ΔG	ΔE	ΔG	ΔE	ΔG	ΔE	ΔG	ΔE	ΔG	ΔE	ΔG	ΔE
G·X(WC)	0.00	0.00	0.00	0.00	0.00	0.00	0.00	0.00	0.00	0.00	0.00	0.00	0.00	0.00	0.00	0.00
G*·X*(L)	8.24	7.89	1.81	1.81	9.44	8.84	2.63	2.29	8.74	8.39	2.09	2.08	9.98	9.39	2.98	2.64
$\mathbf{TS_{G\cdot X(WC)\leftrightarrow G^*\cdot X^*(L)}}$	9.73	13.06	5.03	7.52	8.93	9.96	6.04	9.28	10.35	13.68	5.51	7.99	9.21	10.24	6.56	9.80
$\mathbf{G\cdot X^*_{\uparrow}(w)}$	12.94	13.69	4.54	5.66	11.59	12.06	2.82	3.63	13.35	14.10	4.85	5.97	12.08	12.55	3.20	4.01
$\mathbf{G^*\cdot X_{\uparrow}(w)}$	13.29	15.66	14.53	16.56	11.10	13.05	12.47	14.39	14.85	17.22	15.78	17.81	12.64	14.59	13.7	15.62
$\mathbf{G\cdot X^*_{\downarrow}(w)}$	14.31	15.19	7.61	8.96	12.87	14.24	4.72	6.34	15.08	15.96	8.08	9.42	14.11	15.48	5.28	6.89
$\mathbf{G^*\cdot X_{\downarrow}(w)}$	14.31	15.70	11.51	11.65	13.28	14.54	11.44	11.40	15.10	16.49	11.62	11.76	14.14	15.40	11.5	11.55
$\mathbf{TS^{G^+\cdot X^-}_{G\cdot X(WC)\leftrightarrow G\cdot X^*\uparrow(w)}}$	30.65	30.92	22.06	22.37	31.55	31.93	22.29	22.61	30.47	30.74	21.77	22.08	31.35	31.73	21.9	22.30
$\mathbf{TS^{G^-\cdot X^+}_{G^*\cdot X^*(L)\leftrightarrow G\cdot X^*\downarrow(w)}}$	31.14	31.67	32.06	32.44	24.45	24.74	24.85	25.09	30.88	31.41	31.44	31.83	24.31	24.59	24.4	24.67

For the detailed designations see footnotes of the Table S2.

Table S9. Interbase interaction energies (in kcal·mol^{-1}) for the investigated DNA base pairs and TSs of their conversions *via* the sequential DPT accompanied with structural rearrangements of the bases relative to each other obtained at the MP2/6-311++G(3df,2pd)//B3LYP/6-311++G(d,p) level of theory (ε=1).

Complex	$-\Delta E_{int}$[a]	ΣE_{HB}[b]	$\Sigma E_{HB}/\lvert\Delta E_{int}\rvert$, %	$-\Delta G_{int}$[c]
G·C(WC)[26]	29.28	17.79	60.8	15.97
G*·C*(L)[26]	22.94	19.62	85.5	10.09
G·C*$_{\uparrow}$(w)	15.84	11.14	70.3	4.00
G*·C$_{\uparrow}$(w)	12.57	9.45	75.2	1.72
G·C*$_{\downarrow}$(w)	13.19	9.68	73.4	1.49
G*·C$_{\downarrow}$(w)	12.45	10.17	81.7	0.62
G*·C*$_{O2\uparrow}$(w)	27.74	22.01	79.4	16.37
TS$^{G-\cdot C+}_{G^*\cdot C^*(L)\leftrightarrow G^*\cdot C\uparrow(w)}$	120.13	17.97	15.0	108.20
G*$_{NH3}$·C$_{\downarrow}$(w)	39.14	18.01	46.0	25.10
TS$^{G+\cdot C-}_{G\cdot C(WC)\leftrightarrow G^*\cdot C\downarrow(w)}$	146.26	25.52	17.4	130.93
TS$^{G+\cdot C-}_{G\cdot C(WC)\leftrightarrow G\cdot C^*\uparrow(w)}$	140.58	18.53	13.2	125.07
TS$^{G-\cdot C+}_{G^*\cdot C^*(L)\leftrightarrow G\cdot C^*\downarrow(w)}$	110.53	12.59	11.4	98.36
G*$_{N1}$·C*$_{\downarrow}$(w)	25.39	17.45	68.7	13.16

For the detailed designations see footnotes of the Table S3.

Table S10. Exhaustive energetic and kinetic parameters of the G·C(WC)↔G·C*$_{\uparrow}$(w), G·C(WC)↔G*·C$_{\downarrow}$(w), G*·C*(L)↔G·C*$_{\downarrow}$(w), G·C(WC)↔G·C*$_{\downarrow}$(w), G*·C*(L)↔G*·C$_{\uparrow}$(w), G·C(WC)↔G*·C$_{\uparrow}$(w) and G·C(WC)↔G*·C*(L) DPT tautomerisations producing mutagenic tautomers of the G and C DNA bases. SP calculations are performed at the MP2/6-311++G(2df,pd) and MP2/aug-cc-pVDZ levels of theory for the geometry calculated at the B3LYP/6-311++G(d,p) level of theory in the continuum with ε=1/ε=4.

Level of theory	ΔG[a]	ΔE[b]	ΔΔG$_{TS}$[c]	ΔΔE$_{TS}$[d]	ΔΔG[e]	ΔΔE[f]	τ$_{99.9\%}$[g]	τ[h]
G·C(WC)↔G·C*$_{\uparrow}$(w)								
ε=1 (ν$_i$=169.2*i* cm^{-1})								
MP2/6-311++G(2df,pd)	12.94	13.69	30.65	30.92	17.71	17.23	10.66	1.54
MP2/aug-cc-pVDZ	13.35	14.10	30.47	30.74	17.13	16.64	3.95	0.57
ε=4 (ν$_i$=164.0*i* cm^{-1})								
MP2/6-311++G(2df,pd)	11.59	12.06	31.55	31.93	19.96	19.87	475.94	68.90
MP2/aug-cc-pVDZ	12.08	12.55	31.35	31.73	19.27	19.18	148.66	21.52
G·C(WC)↔G*·C$_{\downarrow}$(w)								
ε=1 (ν$_i$=145.8*i* cm^{-1})								
MP2/6-311++G(2df,pd)	14.31	15.70	30.49	30.94	16.18	15.24	0.81	0.12
MP2/aug-cc-pVDZ	15.10	16.49	31.08	31.53	15.98	15.04	0.58	$8.36\cdot10^{-2}$
ε=4 (ν$_i$=96.3*i* cm^{-1})								
MP2/6-311++G(2df,pd)	13.28	14.54	32.02	31.91	18.74	17.37	61.31	8.88
MP2/aug-cc-pVDZ	14.14	15.40	32.50	32.40	18.36	16.99	32.45	4.70
G·C(WC)↔G*·C*(L)[26]								
ε=1 (ν$_i$=969.0*i* cm^{-1})								
MP2/6-311++G(2df,pd)	8.22	7.87	9.05	13.02	0.83	5.15	$9.61\cdot10^{-12}$	$1.04\cdot10^{-12}$
MP2/aug-cc-pVDZ	8.74	8.39	10.35	13.68	1.62	5.29	$9.25\cdot10^{-12}$	$1.34\cdot10^{-12}$
ε=4 (ν$_i$=727.2*i* cm^{-1})								
MP2/6-311++G(2df,pd)	9.44	8.84	8.93	9.96	-0.51	1.11	$3.17\cdot10^{-13}$	$4.59\cdot10^{-14}$
MP2/aug-cc-pVDZ	9.98	9.39	9.21	10.24	-0.77	0.85	$2.04\cdot10^{-13}$	$2.95\cdot10^{-14}$
G*·C*(L)↔G·C*$_{\downarrow}$(w)								
ε=1 (ν$_i$=190.5*i* cm^{-1})								
MP2/6-311++G(2df,pd)	6.07	7.30	22.90	23.77	16.83	16.47	2.39	0.35
MP2/aug-cc-pVDZ	6.34	7.57	22.15	23.02	15.81	15.45	0.42	$6.12\cdot10^{-2}$
ε=4 (ν$_i$=117.3*i* cm^{-1})								
MP2/6-311++G(2df,pd)	3.43	5.40	15.01	15.89	11.58	10.50	$3.44\cdot10^{-4}$	$5.00\cdot10^{-5}$
MP2/aug-cc-pVDZ	4.12	6.09	14.32	15.20	10.20	9.11	$3.35\cdot10^{-5}$	$4.85\cdot10^{-6}$
G·C(WC)↔G·C*$_{\downarrow}$(w)								
ε=1 (ν$_i$=190.5*i* cm^{-1})								
MP2/6-311++G(2df,pd)	14.31	15.19	31.14	31.67	16.83	16.47	2.39	0.35
MP2/aug-cc-pVDZ	15.08	15.96	30.88	31.41	15.81	15.45	0.42	$6.12\cdot10^{-2}$
ε=4 (ν$_i$=117.3*i* cm^{-1})								
MP2/6-311++G(2df,pd)	12.87	14.24	24.45	24.74	11.58	10.50	$3.45\cdot10^{-4}$	$5.00\cdot10^{-5}$
MP2/aug-cc-pVDZ	14.11	15.48	24.31	24.59	10.20	9.11	$3.35\cdot10^{-5}$	$4.85\cdot10^{-6}$
G*·C*(L)↔G*·C$_{\uparrow}$(w)								
ε=1 (ν$_i$=85.9*i* cm^{-1})								
MP2/6-311++G(2df,pd)	5.05	7.77	16.09	17.20	11.04	9.43	$1.38\cdot10^{-4}$	$2.00\cdot10^{-5}$
MP2/aug-cc-pVDZ	6.11	8.83	16.14	17.25	10.03	8.42	$2.50\cdot10^{-5}$	$3.61\cdot10^{-6}$
ε=4 (ν$_i$=76.0*i* cm^{-1})								
MP2/6-311++G(2df,pd)	1.66	4.21	9.31	9.67	7.65	5.47	$4.26\cdot10^{-7}$	$6.54\cdot10^{-8}$
MP2/aug-cc-pVDZ	2.66	5.20	9.31	9.67	6.66	4.47	$8.36\cdot10^{-8}$	$1.22\cdot10^{-8}$
G·C(WC)↔G*·C$_{\uparrow}$(w)								
ε=1 (ν$_i$=85.9*i* cm^{-1})								
MP2/6-311++G(2df,pd)	13.29	15.66	24.33	25.09	11.04	9.43	$1.38\cdot10^{-4}$	$2.00\cdot10^{-5}$
MP2/aug-cc-pVDZ	14.85	17.22	24.87	25.64	10.03	8.42	$2.50\cdot10^{-5}$	$3.61\cdot10^{-6}$
ε=4 (ν$_i$=76.0*i* cm^{-1})								
MP2/6-311++G(2df,pd)	11.10	13.05	18.75	18.52	7.65	5.47	$4.52\cdot10^{-7}$	$6.54\cdot10^{-8}$
MP2/aug-cc-pVDZ	12.64	14.59	19.30	19.06	6.66	4.47	$8.45\cdot10^{-8}$	$1.22\cdot10^{-8}$

For the detailed designations see footnotes of the Table S4. See also summary Table S7 for the Gibbs and electronic energies of the mispairs and TSs relatively the global minimum – the G·C(WC) DNA base pair.

Table S11. Exhaustive energetic and kinetic parameters of the G·P(WC)↔G·P*$_{\uparrow}$(w), G*·P*(L)↔G·P*$_{\downarrow}$(w), G·P(WC)↔G·P*$_{\downarrow}$(w) and G·P(WC)↔G*·P*(L) DPT tautomerisations producing mutagenic tautomers of the mutagenic analogue of C DNA base – P. SP calculations are performed at the MP2/6-311++G(2df,pd) and MP2/aug-cc-pVDZ levels of theory for the geometry calculated at the B3LYP/6-311++G(d,p) level of theory in the continuum with ε=1/ε=4.

Level of theory	ΔG	ΔE	$\Delta\Delta G_{TS}$	$\Delta\Delta E_{TS}$	ΔΔG	ΔΔE	$\tau_{99.9\%}$	τ
G·P(WC)↔G·P*$_{\uparrow}$(w)								
ε=1 (ν_i=140.5*i* cm^{-1})								
MP2/6-311++G(2df,pd)	4.54	5.66	22.06	22.37	17.52	16.71	7.75	1.12
MP2/aug-cc-pVDZ	4.85	5.97	21.77	22.08	16.92	16.11	2.80	0.41
ε=4 (ν_i=134.4*i* cm^{-1})								
MP2/6-311++G(2df,pd)	2.82	3.63	22.29	22.61	19.47	18.98	208.92	30.50
MP2/aug-cc-pVDZ	3.20	4.01	21.99	22.30	18.78	18.29	65.37	9.51
G·P(WC)↔G*·P*(L)								
ε=1 (ν_i=1180.3*i* cm^{-1})								
MP2/6-311++G(2df,pd)	1.81	1.81	5.03	7.52	3.22	5.71	$1.09\cdot10^{-10}$	$1.65\cdot10^{-11}$
MP2/aug-cc-pVDZ	2.09	2.08	5.51	7.99	3.42	5.91	$1.55\cdot10^{-10}$	$2.31\cdot10^{-11}$
ε=4 (ν_i=1258.6*i* cm^{-1})								
MP2/6-311++G(2df,pd)	2.63	2.29	6.04	9.28	3.41	6.99	$1.44\cdot10^{-10}$	$2.11\cdot10^{-11}$
MP2/aug-cc-pVDZ	2.98	2.64	6.56	9.80	3.58	7.15	$1.93\cdot10^{-10}$	$2.81\cdot10^{-11}$
G*·P*(L)↔G·P*$_{\downarrow}$(w)								
ε=1 (ν_i=158.1*i* cm^{-1})								
MP2/6-311++G(2df,pd)	5.80	7.15	30.24	30.64	24.44	23.49	$9.24\cdot10^{5}$	$1.34\cdot10^{5}$
MP2/aug-cc-pVDZ	5.99	7.34	29.35	29.75	23.36	22.40	$1.48\cdot10^{5}$	$2.15\cdot10^{4}$
ε=4 (ν_i=113.8*i* cm^{-1})								
MP2/6-311++G(2df,pd)	2.09	4.05	22.21	22.80	20.12	18.75	$6.14\cdot10^{2}$	91.51
MP2/aug-cc-pVDZ	2.29	4.25	21.45	22.03	19.15	17.78	$1.21\cdot10^{2}$	17.85
G·P(WC)↔G·P*$_{\downarrow}$(w)								
ε=1 (ν_i=158.1*i* cm^{-1})								
MP2/6-311++G(2df,pd)	7.61	8.96	32.06	32.44	24.44	23.49	$9.24\cdot10^{5}$	$1.34\cdot10^{5}$
MP2/aug-cc-pVDZ	8.08	9.42	31.44	31.83	23.36	22.40	$1.48\cdot10^{5}$	$2.15\cdot10^{4}$
ε=4 (ν_i=113.8*i* cm^{-1})								
MP2/6-311++G(2df,pd)	4.72	6.34	24.85	25.09	20.12	18.75	$6.32\cdot10^{2}$	91.51
MP2/aug-cc-pVDZ	5.28	6.89	24.43	24.67	19.15	17.78	$1.23\cdot10^{2}$	17.85

For the designations see footnotes of the Table S4. See also summary Table S8 for the comparative Gibbs and electronic energies of the mispairs and TSs relatively the global minima – the G·C(WC) and G·P(WC) Watson-Crick-like base pairs.

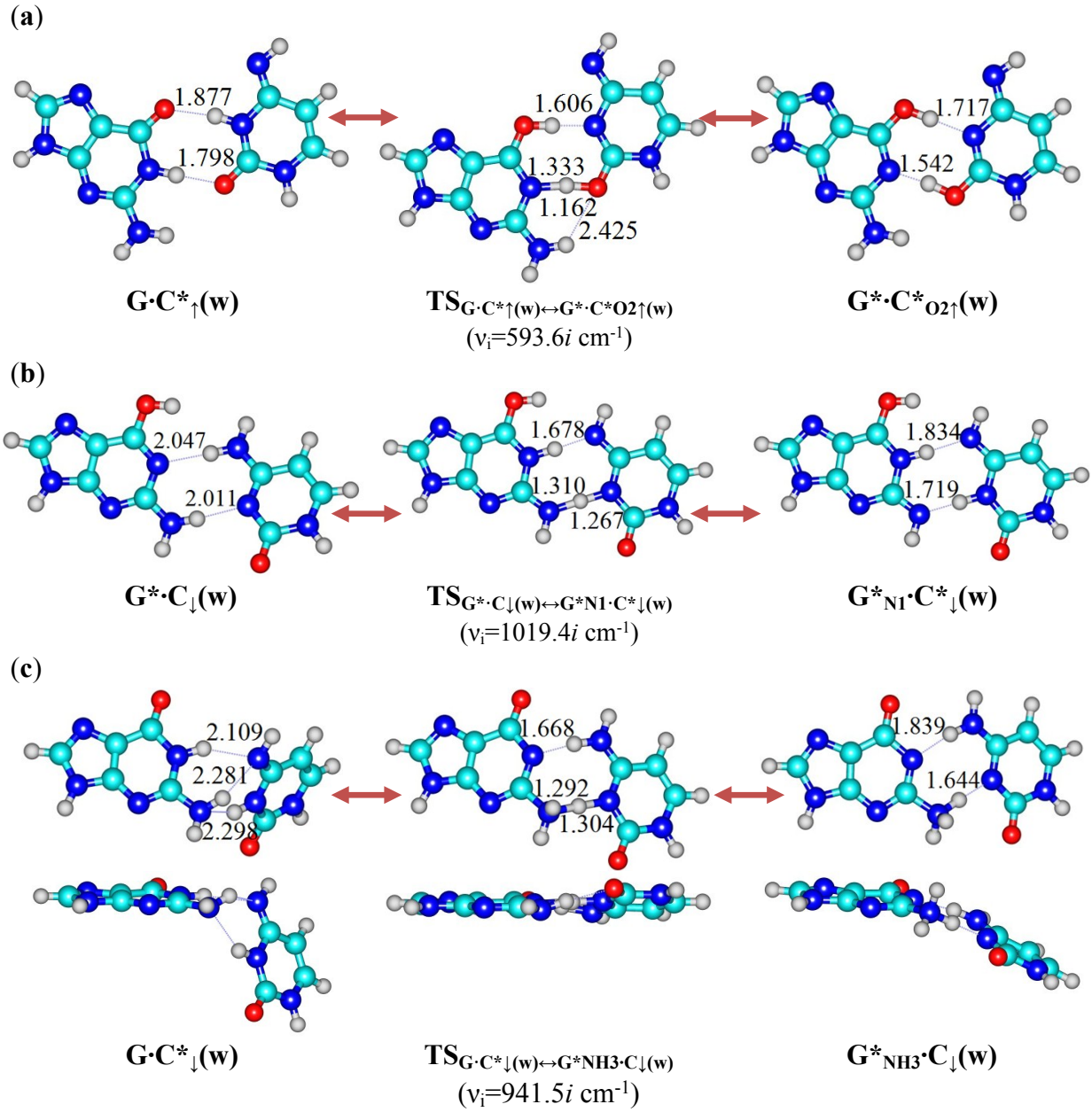

Figure S5. Structures corresponding to the stationary points on the reaction pathways of the (**a**) G·C*$_{\uparrow}$(w)↔G*·C*$_{O2\uparrow}$(w), (**b**) G*·C$_{\downarrow}$(w)↔G*$_{N1}$·C*$_{\downarrow}$(w) and (**c**) G·C*$_{\downarrow}$(w)↔G*$_{NH3}$·C$_{\downarrow}$(w) tautomerisations *via* the asynchronous concerted DPT along the neighboring H-bonds accompanied with structural rearrangements of the bases relative to each other obtained at the B3LYP/6-311++G(d,p) level of theory (ε=1). Perpendicular projections of the non-planar complexes are given below them. For the detailed designations see Fig. S2 caption; for more detailed physico-chemical characteristics of the H-bonds see Table S6.

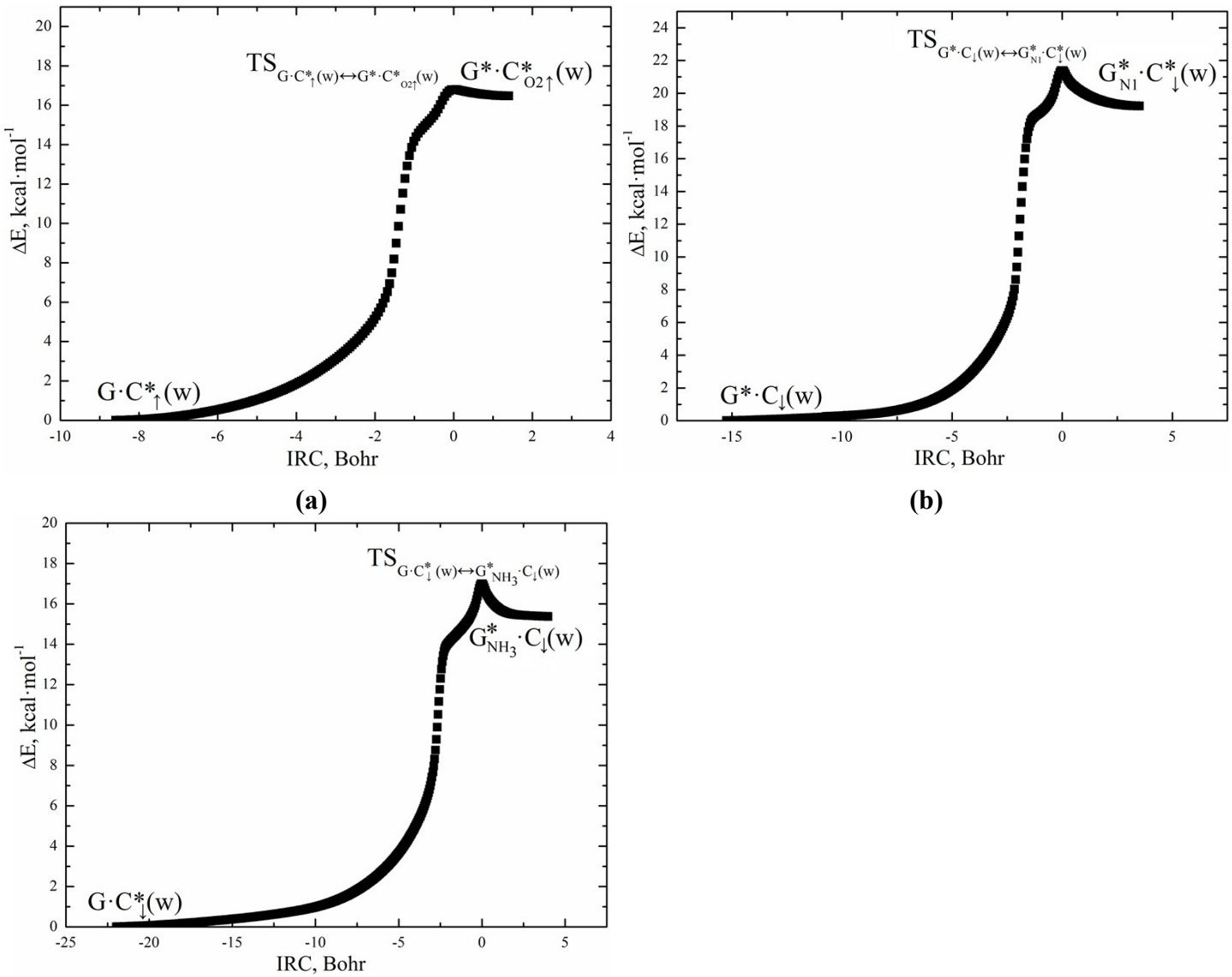

Figure S6. Profiles of the relative electronic energy ΔE of the DNA base mispairs along the IRC of the (**a**) G·C*$_{\uparrow}$(w)↔G*·C*$_{O2\uparrow}$(w), (**b**) G*·C$_{\downarrow}$(w)↔G*$_{N1}$·C*$_{\downarrow}$(w) and (**c**) G·C*$_{\downarrow}$(w)↔G*$_{NH3}$·C$_{\downarrow}$(w) tautomerisations *via* the sequential DPT accompanied with structural rearrangements of the bases relative to each other. Presented data are obtained by following IRC at the B3LYP/6-311++G(d,p) level of theory in the continuum with ε=1.

Table S12. Exhaustive energetic and kinetic parameters of the $G{\cdot}C^*_{\uparrow}(w){\leftrightarrow}G^*{\cdot}C^*_{O2\uparrow}(w)$, $G^*{\cdot}C_{\downarrow}(w){\leftrightarrow}G^*_{N1}{\cdot}C^*_{\downarrow}(w)$ and $G{\cdot}C^*_{\downarrow}(w){\leftrightarrow}G^*_{NH3}{\cdot}C_{\downarrow}(w)$ tautomerisations *via* the DPT accompanied with structural rearrangements of the bases relative to each other along neighboring H-bonds. SP calculations are performed at the MP2/6-311++G(2df,pd) and MP2/aug-cc-pVDZ levels of theory for the geometry calculated at the B3LYP/6-311++G(d,p) level of theory (ε=1).

Level of theory	ΔG	ΔE	$\Delta\Delta G_{TS}$	$\Delta\Delta E_{TS}$	ΔΔG	ΔΔE	$\tau_{99.9\%}$	τ
$G{\cdot}C^*_{\uparrow}(w){\leftrightarrow}G^*{\cdot}C^*_{O2\uparrow}(w)$ (ν_i=593.6*i* cm^{-1})								
MP2/6-311++G(2df,pd)	11.33	12.26	9.98	12.73	-1.35	0.47	$8.60{\cdot}10^{-14}$	$1.25{\cdot}10^{-14}$
MP2/aug-cc-pVDZ	11.91	12.84	10.62	13.37	-1.29	0.53	$9.51{\cdot}10^{-14}$	$1.38{\cdot}10^{-14}$
$G^*{\cdot}C_{\downarrow}(w){\leftrightarrow}G^*_{N1}{\cdot}C^*_{\downarrow}(w)$ (ν_i=1019.4*i* cm^{-1})								
MP2/6-311++G(2df,pd)	20.23	20.44	18.71	21.42	-1.52	0.98	$4.41{\cdot}10^{-14}$	$6.38{\cdot}10^{-15}$
MP2/aug-cc-pVDZ	19.48	19.69	18.02	20.73	-1.45	1.05	$4.93{\cdot}10^{-14}$	$7.14{\cdot}10^{-15}$
$G{\cdot}C^*_{\downarrow}(w){\leftrightarrow}G^*_{NH3}{\cdot}C_{\downarrow}(w)$ (ν_i=941.5*i* cm^{-1})								
MP2/6-311++G(2df,pd)	13.18	12.46	12.77	14.02	-0.41	1.55	$3.11{\cdot}10^{-13}$	$4.50{\cdot}10^{-14}$
MP2/aug-cc-pVDZ	12.08	11.36	11.88	13.13	-0.20	1.76	$4.43{\cdot}10^{-13}$	$6.42{\cdot}10^{-14}$

For the designations see footnotes of the Table S4. See also summary Table S7 for the Gibbs and electronic energies of the mispairs and TSs relatively the global minimum – the G·C(WC) Watson-Crick DNA base pair.

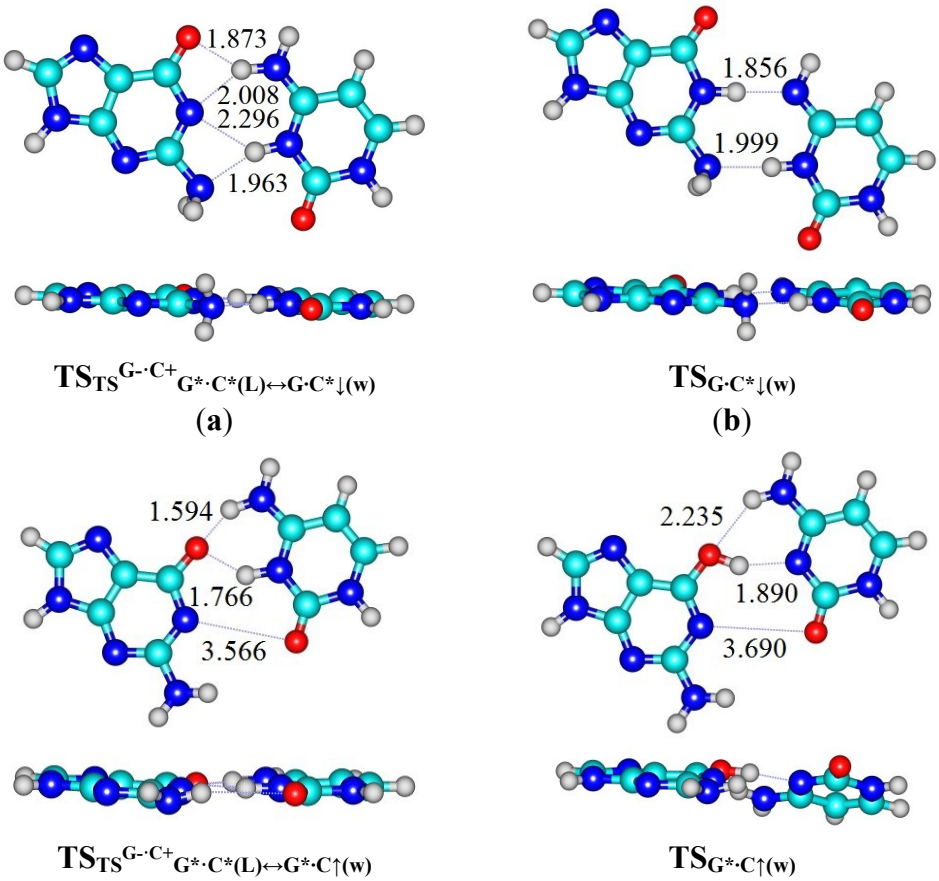

$TS_{TS}^{G-\cdot C+}{}_{G^*\cdot C^*(L)\leftrightarrow G\cdot C^*\downarrow(w)}$ (**a**)

$TS_{G\cdot C^*\downarrow(w)}$ (**b**)

$TS_{TS}^{G-\cdot C+}{}_{G^*\cdot C^*(L)\leftrightarrow G^*\cdot C\uparrow(w)}$ (**c**)

$TS_{G^*\cdot C\uparrow(w)}$ (**d**)

Figure S7. Transition states of the conformational interconversions of the mirror-symmetric enantiomers of the (**a**) $TS^{G-\cdot C+}{}_{G^*\cdot C^*(L)\leftrightarrow G\cdot C^*\downarrow(w)}$, (**b**) $G\cdot C^*{}_{\downarrow}(w)$, (**c**) $TS_{TS}^{G-\cdot C+}{}_{G^*\cdot C^*(L)\leftrightarrow G^*\cdot C\uparrow(w)}$ and (**d**) $G^*\cdot C_{\uparrow}(w)$ biologically important complexes obtained at the B3LYP/6-311++G(d,p) level of theory in the continuum with ε=1. For the designations see Fig. S2 caption.

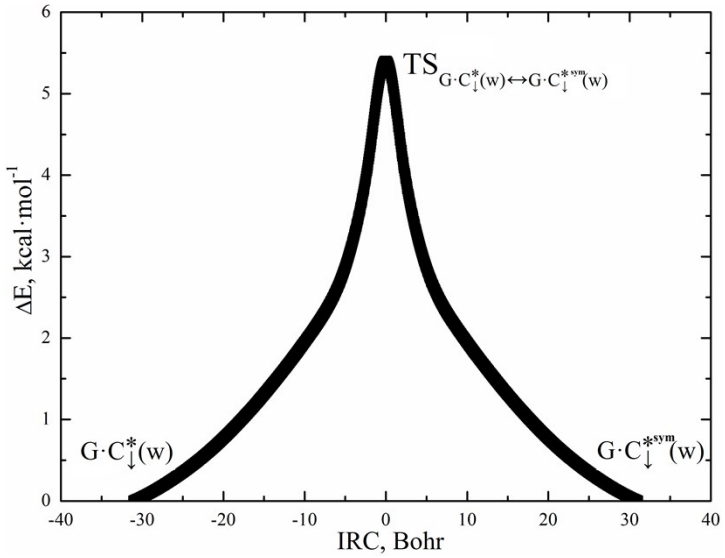

Figure S8. Profile of the relative electronic energy ΔE of the conformational interconversion of the mirror-symmetric enantiomers of the wobble G·C*↓(w) DNA base mispair *via* the rotation of the NH_2 amino group of the G base around the C2N2 covalent bond along the IRC obtained at the B3LYP/6-311++G(d,p) level of theory (ε=1).

Table S13. Energetic and kinetic characteristics of the conformational interconversions of the mirror-symmetric enantiomers of the biologically important and significantly non-planar DNA base mispairs and TSs of their planarization calculated at the MP2/aug-cc-pVDZ//B3LYP/6-311++G(d,p) level of theory (ε=1) (see also Figs. S7 and S8).

Transition state of the interconversion	$\Delta\Delta G_{TS}$[a]	$\Delta\Delta E_{TS}$[b]	$\tau_{99.9\%}$[c]	ν_i[d]	β[e]
$\mathbf{TS_{TS}^{G\text{-}\cdot C+}}_{\mathbf{G^*\cdot C^*(L)\leftrightarrow G\cdot C^*\downarrow(w)}}$	2.56	2.58	$4.17\cdot10^{-11}$	91.6*i*	∠C6N1(G^+)N3C4(C^-)=±38.0
$\mathbf{TS_{G\cdot C^*\downarrow(w)}}$	4.71	4.12	$1.583\cdot10^{-9}$	188.4*i*	∠N1C2(G)N3C4(C*)=±42.3
$\mathbf{TS_{TS}^{G\text{-}\cdot C+}}_{\mathbf{G^*\cdot C^*(L)\leftrightarrow G^*\cdot C\uparrow(w)}}$	3.25	2.14	$1.33\cdot10^{-10}$	26.3*i*	∠C6N1(G^-)N3C4(C^+)=±40.2
$\mathbf{TS_{G^*\cdot C\uparrow(w)}}$	1.68	0.76	$9.48\cdot10^{-12}$	10.6*i*	∠C6N1(G*)N1C6(C)=±31.0

[a]The Gibbs free energy barrier of the conformational interconversion under normal conditions, kcal·mol^{-1}; [b]The electronic energy barrier of the conformational interconversion, kcal·mol^{-1}; [c]The time necessary to reach 99.9% of the equilibrium concentration between the mirror-symmetric enantiomers, s; [d]Imaginary frequency in the transition state of the conformational interconversion, cm^{-1}; [e]Dihedral angle that characterize the non-planarity of the complex, °; signs "±" correspond to the mirror-symmetric enantiomers.

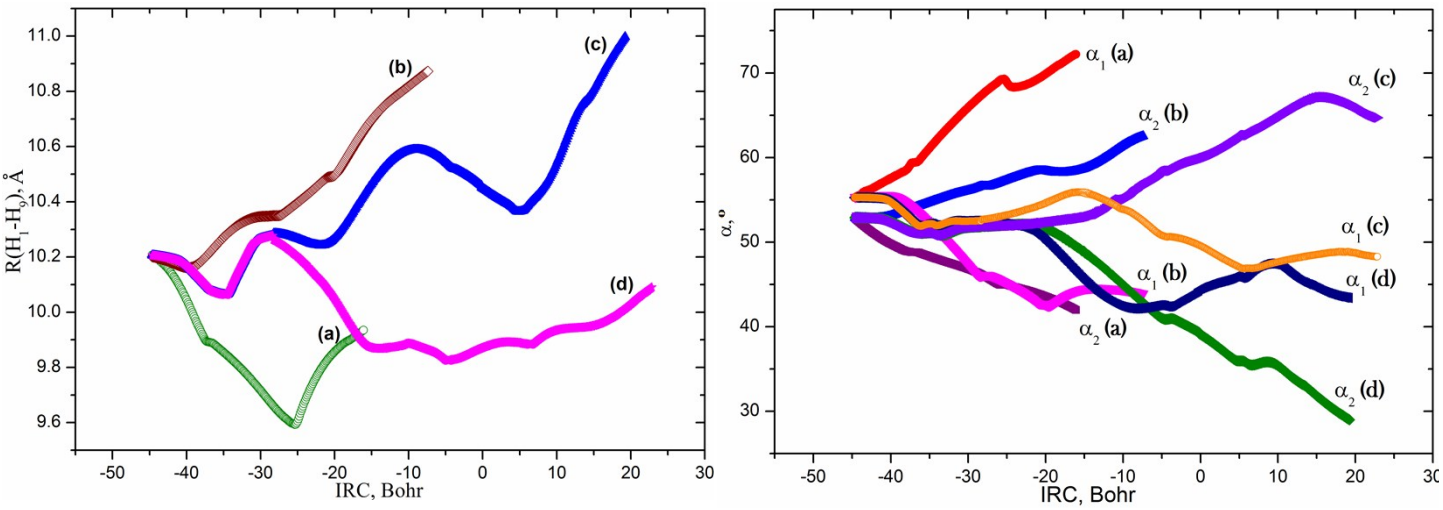

Figure S9. Profiles of the $R(H_1\text{-}H_9)$ distances between the H_1 and H_9 glycosidic hydrogens and the α_1 ($\angle N1H_1(C)H_9(G)$) or α_2 ($\angle N9H_9(G)H_1(C)$) glycosidic angles of the C and G bases, respectively, along the IRC of the (**a**) $G{\cdot}C(WC){\leftrightarrow}G{\cdot}C^*_{\uparrow}(w)$, (**b**) $G{\cdot}C(WC){\leftrightarrow}G^*{\cdot}C_{\downarrow}(w)$, (**c**) $G{\cdot}C(WC){\leftrightarrow}G^*{\cdot}C^*(L){\leftrightarrow}G{\cdot}C^*_{\downarrow}(w)$ and (**d**) $G{\cdot}C(WC){\leftrightarrow}G^*{\cdot}C^*(L){\leftrightarrow}G^*{\cdot}C_{\uparrow}(w)$ tautomerisations *via* the sequential DPT accompanied with structural rearrangements (B3LYP/6-311++G(d,p) level of theory (ε=1)) (see also Figs. 5, 7). Continuity of the depicted dependencies and range of their changes unequivocally points to the non-dissociative nature of the tautomerisation processes.

Table S14. Patterns of the specific intermolecular interactions including AH···B H-bonds and loosened A-H-B covalent bridges that sequentially replace each other along the IRC of the biologically important (a) G·C(WC)↔G·C*$_{\uparrow}$(w), (b) G·C(WC)↔G*·C$_{\downarrow}$(w), (c) G·C(WC)↔G*·C*(L)↔G·C*$_{\downarrow}$(w) and (d) G·C(WC)↔G*·C*(L)↔G*·C$_{\uparrow}$(w) tautomerisations *via* the sequential DPT and their ranges of the existence obtained at the B3LYP/6-311++G(d,p) level of theory (ε=1) (see also Figs. 5 and 8).

Patterns	IRC range, Bohr	Intermolecular interactions, forming patterns
G·C(WC)↔G·C*$_{\uparrow}$(w)		
I	[-13.50÷-7.95)	(C)N4H···O6(G), (G)N1H···N3(C), (G)N2H···O2(C)
II	[-7.95÷-7.23)	(C)N4H···O6(G), (G)N1H···N3(C), (G)N2H···O2(C), (G)O6···N3(C)
III	[-7.23÷-5.68)	(C)N4H···O6(G), (G)N1H···N3(C), (G)N2H···O2(C)
IV	[-5.68÷-5.20)	(C)N4-H-O6(G), (G)N1H···N3(C), (G)N2H···O2(C)
V	[-5.20÷-3.63)	(G)O6H···N4(C), (G)N1H···N3(C), (G)N2H···O2(C)
VI	[-3.63÷-2.90)	(G)O6H···N4(C), (G)N1H···N3(C), (G)N1H···O2(C), (G)N2H···O2(C)
VII	[-2.90÷0.60)	(G)O6H···N4(C), (G)O6H···N3(C), (G)N1H···N3(C), (G)N1H···O2(C), (G)N2H···O2(C)
VIII	[0.60÷1.21)	(G)O6H···N3(C), (G)N1H···N3(C), (G)N1H···O2(C), (G)N2H···O2(C)
IX	[1.21÷4.95)	(G)O6H···N3(C), (G)N1H···O2(C), (G)N2H···O2(C)
X	[4.95÷5.43)	(G)O6-H-N3(C), (G)N1H···O2(C), (G)N2H···O2(C)
XI	[5.43÷11.09)	(C)N3H···O6(G), (G)N1H···O2(C), (G)N2H···O2(C)
XII	[11.09÷15.04]	(C)N3H···O6(G), (G)N1H···O2(C)
G·C(WC)↔G*·C$_{\downarrow}$(w)		
I	[-23.30÷-11.77)	(C)N4H···O6(G), (G)N1H···N3(C), (G)N2H···O2(C)
II	[-11.77÷-9.92)	(C)N4H···O6(G), (G)N1H···N3(C), (G)N2H···N3(C), (G)N2H···O2(C)
III	[-9.92÷-8.17)	(C)N4H···O6(G), (G)N1H···N3(C), (G)N2H···N3(C), (G)N2H···O2(C), (G)H_1···H_4(C)
IV	[-8.17÷-6.97)	(C)N4H···O6(G), (G)N1H···N4(C), (G)N1H···N3(C), (G)N2H···N3(C), (G)N2H···O2(C)
V	[-6.97÷-6.32)	(C)N4H···O6(G), (G)N1H···N4(C), (G)N1H···N3(C), (G)N2H···N3(C)
VI	[-6.32÷-5.89)	(C)N4-H-O6(G), (G)N1H···N4(C), (G)N1H···N3(C), (G)N2H···N3(C)
VII	[-5.89÷-2.94)	(G)O6H···N4(G), (G)N1H···N4(C), (G)N1H···N3(C), (G)N2H···N3(C)
VIII	[-2.94÷0.44)	(G)O6H···N4(G), (G)N1H···N4(C), (G)N2H···N3(C)
IX	[0.44÷0.87)	(G)O6H···N4(G), (G)N1-H-N4(C), (G)N2H···N3(C)
X	[0.87÷5.44)	(G)O6H···N4(G), (C)N4H···N1(G), (G)N2H···N3(C)
XI	[5.44÷13.94]	(C)N4H···N1(G), (G)N2H···N3(C)
G·C(WC)↔G*·C*(L)↔G·C*$_{\downarrow}$(w)		
I	[-44.64÷-35.59)	(C)N4H···O6(G), (G)N1H···N3(C), (G)N2H···O2(C)
II	[-35.59÷-35.16)	(C)N4H···O6(G), (G)N1-H-N3(C), (G)N2H···O2(C)
III	[-35.16÷-34.68)	(C)N4-H-O6(G), (C)N3H···N1(G), (G)N2H···O2(C)
IV	[-34.68÷-9.64)	(G)O6H···N4(C), (C)N3H···N1(G), (G)N2H···O2(C)
V	[-9.64÷-4.16)	(G)O6H···N4(C), (C)N3H···N1(G), (G)N2···O2(C)
VI	[-4.16÷-3.79)	(G)O6-H-N4(C), (C)N3H···N1(G), (G)N2···O2(C)
VII	[-3.79÷-2.56)	(C)N4H···O6(G), (C)N3H···N1(G), (G)N2···O2(C)
VIII	[-2.56÷-1.42)	(C)N4H···O6(G), (C)N3H···N1(G), (C)N3H···N2(G)
IX	[-1.42÷1.51)	(C)N4H···O6(G), (C)N4H···N1(G), (C)N3H···N1(G), (C)N3H···N2(G)
X	[1.51÷2.75)	(C)N4H···N1(G), (C)N3H···N1(G), (C)N3H···N2(G)
XI	[2.75÷5.30)	(C)N4H···N1(G), (C)N3H···N2(G)
XII	[5.30÷5.77)	(C)N4-H-N1(G), (C)N3H···N2(G)
XIII	[5.77÷19.37)	(G)N1H···N4(C), (C)N3H···N2(G)
XIV	[19.37÷20.97)	(G)N1H···N4(C), (G)N2···N4(C), (C)N3H···N2(G)
XV	[20.97÷22.83)	(G)N1H···N4(C), (G)N2H···N4(C), (C)N3H···N2(G)
G·C(WC)↔G*·C*(L)↔G*·C$_{\uparrow}$(w)		
I	[-44.48÷-35.43)	(C)N4H···O6(G), (G)N1H···N3(C), (G)N2H···O2(C)
II	[-35.43÷-35.00)	(C)N4H···O6(G), (G)N1-H-N3(C), (G)N2H···O2(C)
III	[-35.00÷-34.52)	(C)N4-H-O6(G), (C)N3H···N1(G), (G)N2H···O2(C)
IV	[-34.52÷-4.72)	(G)O6H···N4(C), (C)N3H···N1(G), (G)N2H···O2(C)
V	[-4.72÷-3.66)	(G)O6H···N4(C), (C)N3H···O6(G), (C)N3H···N1(G), (G)N2H···O2(C)
VI	[-3.66÷-3.12)	(G)O6-H-N4(C), (C)N3H···O6(G), (C)N3H···N1(G)
VII	[-3.12÷-0.27)	(G)N4H···O6(C), (C)N3H···O6(G), (C)N3H···N1(G)
VIII	[-0.27÷4.75)	(G)N4H···O6(C), (C)N3H···O6(G)
IX	[4.75÷5.15)	(G)N4H···O6(C), (C)N3-H-O6(G)
X	[5.15÷19.39]	(G)N4H···O6(C), (C)O6H···N3(G)

References.

1. Frisch, M.J., Trucks, G.W., Schlegel, H.B., Scuseria, G.E., Robb, M.A., & Cheeseman, J.R., … Pople, J.A. (2010). *GAUSSIAN 09* (Revision B.01). Wallingford CT: Gaussian Inc.
2. Tirado-Rives, J., & Jorgensen, W.L. Performance of B3LYP Density Functional Methods for a large set of organic molecules. *J. Chem. Theory Comput.* **4***,* 297–306 (2008).
3. Parr, R.G., & Yang, W. *Density-functional theory of atoms and molecules*. Oxford: Oxford University Press (1989).
4. Lee, C., Yang, W., & Parr, R.G. Development of the Colle-Salvetti correlation-energy formula into a functional of the electron density. *Phys. Rev. B.* **37**, 785-789 (1988).
5. Matta, C.F. How dependent are molecular and atomic properties on the electronic structure method? Comparison of Hartree-Fock, DFT, and MP2 on a biologically relevant set of molecules. *J. Comput. Chem.* **31**, 1297–1311 (2010).
6. Brovarets', O.O., Zhurakivsky, R.O., & Hovorun, D.M. The physico-chemical mechanism of the tautomerisation *via* the DPT of the long Hyp*·Hyp Watson-Crick base pair containing rare tautomer: a QM and QTAIM detailed look. *Chem. Phys. Lett.* **578**, 126-132 (2013).
7. Brovarets', O.O., & Hovorun, D.M. Atomistic understanding of the C·T mismatched DNA base pair tautomerization *via* the DPT: QM and QTAIM computational approaches. *J. Comput. Chem.* **34**, 2577-2590 (2013).
8. Brovarets', O.O., Zhurakivsky, R.O., & Hovorun, D.M. Is the DPT tautomerisation of the long A·G Watson-Crick DNA base mispair a source of the adenine and guanine mutagenic tautomers? A QM and QTAIM response to the biologically important question. *J. Comput. Chem.* **35**, 451-466 (2014).
9. Samijlenko, S.P., Yurenko, Y.P., Stepanyugin, A.V., & Hovorun, D.M. Tautomeric equilibrium of uracil and thymine in model protein−nucleic acid contacts. Spectroscopic and quantum chemical approach. *J. Phys. Chem. B* **114**, 1454-1461 (2012).
10. Peng, C., Ayala, P.Y., Schlegel, H.B., & Frisch, M.J. Using redundant internal coordinates to optimize equilibrium geometries and transition states. *J. Comput. Chem.* **17**, 49–56 (1996).
11. Atkins, P.W. *Physical chemistry*. Oxford: Oxford University Press (1998).
12. Cossi, M., Rega, N., Scalmani, G., & Barone, V. Energies, structures, and electronic properties of molecules in solution with the C-PCM solvation model. *J. Comput. Chem.* **24**, 669 –681 (2003).
13. Barone, V., & Cossi, M. Quantum calculation of molecular energies and energy gradients in solution by a conductor solvent model. *J. Phys. Chem. A* **102***,* 1995–2001 (1998).
14. Mennucci, B. Polarizable continuum model. *WIREs Comput. Mol. Sci.* **2**, 386–404 (2012).
15. García-Moreno, B.E., Dwyer, J.J., Gittis, A.G., Lattman, E.E., Spencer D.S., & Stites, W.E. Experimental measurement of the effective dielectric in the hydrophobic core of a protein. *Biophys. Chem.* **64**, 211-224 (1997).
16. Brovarets', O. O., Yurenko, Y. P., Dubey, I. Y., & Hovorun, D. M. Can DNA-binding proteins of replisome tautomerize nucleotide bases? *Ab initio* model study. *J. Biomol. Struct. & Dynam.* **29**, 1101–1109 (2012).
17. Bayley, S.T. The dielectric properties of various solid crystalline proteins, amino acids and peptides. *Trans. Faraday Soc.* **47**, 509-517 (1951).
18. Dewar, M.J.S., & Storch, D.M. Alternative view of enzyme reactions. *Proc. Natl. Acad. Sci. USA* **82**, 2225−2229 (1985).
19. Mertz E.L., & Krishtalik, L.I. Low dielectric response in enzyme active site. *Proc. Natl. Acad. Sci. USA* **97**, 2081-2086 (2000).
20. Petrushka, J., Sowers, L.C., & Goodman, M. Comparison of nucleotide interactions in water, proteins, and vacuum: Model for DNA polymerase fidelity. *Proc. Natl. Acad. Sci. USA* **83,** 1559-1562 (1986).

21. Hratchian, H.P., & Schlegel, H.B. (2005). Finding minima, transition states, and following reaction pathways on ab initio potential energy surfaces. In Dykstra, C.E., Frenking, G., Kim, K.S., & Scuseria, G. (Eds.), *Theory and applications of computational chemistry: The first 40 years* (pp. 195-249). Amsterdam: Elsevier.
22. Brovarets', O.O., Zhurakivsky, R.O., & Hovorun, D.M. DPT tautomerisation of the wobble guanine·thymine DNA base mispair is not mutagenic: QM and QTAIM arguments. *J. Biomol. Struct. & Dynam.* **33**, 674-689 (2015).
23. Brovarets', O.O., Zhurakivsky, R.O., & Hovorun, D.M. The physico-chemical "anatomy" of the tautomerisation through the DPT of the biologically important pairs of hypoxanthine with DNA bases: QM and QTAIM perspectives. *J. Mol. Model.* **19**, 4119-4137 (2013).
24. Frisch, M.J., Head-Gordon, M., & Pople, J.A. Semi-direct algorithms for the MP2 energy and gradient. *Chem. Phys. Lett.* **166***,* 281-289 (1990).
25. Hariharan, P.C., & Pople, J.A. The influence of polarization functions on molecular orbital hydrogenation energies. *Theor. Chim. Acta* **28**, 213−222 (1973).
26. Krishnan, R., Binkley, J.S., Seeger, R., & Pople, J.A. Self-consistent molecular orbital methods. XX. A basis set for correlated wave functions. *J. Chem. Phys.* **72**, 650−654 (1980).
27. Kendall, R.A., Dunning, Jr., T.H., & Harrison, R.J. Electron affinities of the first-row atoms revisited. Systematic basis sets and wave functions. *J. Chem. Phys.* **96**, 6796−6806 (1992).
28. Boys, S.F., & Bernardi, F. The calculation of small molecular interactions by the differences of separate total energies. Some procedures with reduced errors. *Mol. Phys.* **19***,* 553–566 (1970).
29. Gutowski, M., Van Lenthe, J.H., Verbeek, J., Van Duijneveldt, F.B., & Chalasinski, G. The basis set superposition error in correlated electronic structure calculations*. Chem. Phys. Lett.* **124***,* 370–375 (1986).
30. Sordo, J.A., Chin, S., & Sordo, T.L. (1988). On the counterpoise correction for the basis set superposition error in large systems. *Theor. Chim. Acta* **74**, 101–110 (1988).
31. Sordo, J.A. On the use of the Boys–Bernardi function counterpoise procedure to correct barrier heights for basis set superposition error. *J. Mol. Struct.* **537***,* 245–251 (2001).
32. Wigner, E. Über das Überschreiten von Potentialschwellen bei chemischen Reaktionen [Crossing of potential thresholds in chemical reactions]. *Zeits. Physik. Chem.* **B19**, 203−216 (1932).
33. Brovarets', O.O., & Hovorun, D.M. Atomistic nature of the DPT tautomerisation of the biologically important C·C* DNA base mispair containing amino and imino tautomers of the cytosine: A QM and QTAIM approach. *Phys. Chem. Chem. Phys.* **15**, 20091-20104 (2013).
34. Brovarets', O.O., & Hovorun, D.M. DPT tautomerisation of the $G{\cdot}A_{syn}$ and $A^{*}{\cdot}G^{*}_{syn}$ DNA mismatches: A QM/QTAIM combined atomistic investigation. *Phys. Chem. Chem. Phys*. **16**, 9074-9085 (2014).
35. Bader, R.F.W. (1990). *Atoms in molecules: A quantum theory*. Oxford: Oxford University Press.
36. Matta, C.F. Modeling biophysical and biological properties from the characteristics of the molecular electron density, electron localization and delocalization matrices, and the electrostatic potential. *J. Comput. Chem.* **35***,* 1165-1198 (2014).
37. Lecomte, C., Espinosa, E., & Matta, C.F. On atom–atom 'short contact' bonding interactions in crystals. *IUCrJ* **2**, 161–163 (2015).
38. Matta, C.F., Huang L., & Masaa, L. Characterization of a trihydrogen bond on the basis of the topology of the electron density. *J. Phys. Chem. A* **115**, 12451-12458 (2011).
39. Keith, T.A. (2010). *AIMAll* (Version 10.07.01). Retrieved from aim.tkgristmill.com.
40. Brovarets', O. O., Yurenko, Y. P., & Hovorun, D. M. Intermolecular CH···O/N H-bonds in the biologically important pairs of natural nucleobases: A thorough quantum-chemical study. *J. Biomol. Struct. & Dynam.* **32***,* 993-1022 (2014).
41. Brovarets', O. O., Yurenko, Y. P., & Hovorun, D. M. The significant role of the intermolecular CH···O/N hydrogen bonds in governing the biologically important pairs of the DNA and RNA modified bases: a comprehensive theoretical investigation. *J. Biomol. Struct. & Dynam.* **33**, 1624-1652 (2015).

42. Matta, C.F., Castillo, N., & Boyd, R.J. Extended weak bonding interactions in DNA: π-stacking (base-base), base-backbone, and backbone-backbone interactions. *J. Phys. Chem. B* **110**, 563-578 (2006).
43. Espinosa, E., Molins, E., & Lecomte, C. Hydrogen bond strengths revealed by topological analyses of experimentally observed electron densities. *Chem. Phys. Lett.* **285**, 170–173 (1998).
44. Mata, I., Alkorta, I., Espinosa, E., & Molins, E. Relationships between interaction energy, intermolecular distance and electron density properties in hydrogen bonded complexes under external electric fields. *Chem. Phys. Lett.* **507**, 185–189 (2011).
45. Iogansen, A.V. Direct proportionality of the hydrogen bonding energy and the intensification of the stretching *ν*(XH) vibration in infrared spectra. *Spectrochim. Acta Part A: Mol. Biomol. Spectrosc.* **55***,* 1585–1612 (1999).
46. Brovarets', O.O., Zhurakivsky, R.O., & Hovorun, D.M. Does the tautomeric status of the adenine bases change under the dissociation of the A*·A_{syn} Topal-Fresco DNA mismatch? A combined QM and QTAIM atomistic insight. *Phys. Chem. Chem. Phys.* **16**, 3715-3725 (2014).
47. Brovarets', O.O., & Hovorun, D.M. How the long G·G* Watson-Crick DNA base mispair comprising keto and enol tautomers of the guanine tautomerises? The results of the QM/QTAIM investigation. *Phys. Chem. Chem. Phys.* **6**, 15886-15899 (2014).
48. Brovarets', O.O., & Hovorun, D.M. Does the G·G^*_{syn} DNA mismatch containing canonical and rare tautomers of the guanine tautomerise through the DPT? A QM/QTAIM microstructural study. *Mol. Phys.* **112**, 3033-3046 (2014).
49. Nikolaienko, T.Y., Bulavin, L.A., & Hovorun, D.M. Bridging QTAIM with vibrational spectroscopy: The energy of intramolecular hydrogen bonds in DNA-related biomolecules. *Phys. Chem. Chem. Phys.* **14**, 7441–7447 (2012).
50. Saenger, W. (1984). *Principles of nucleic acid structure.* New York: Springer.
51. Brovarets', O.O., Zhurakivsky, R.O., & Hovorun, D.M. DPT tautomerization of the long A·A* Watson-Crick base pair formed by the amino and imino tautomers of adenine: combined QM and QTAIM investigation. *J. Mol. Model.* **19**, 4223-4237 (2013).
52. Brovarets', O.O., Zhurakivsky, R.O., & Hovorun, D.M. Does the tautomeric status of the adenine bases change under the dissociation of the A*·A_{syn} Topal-Fresco DNA mismatch? A combined QM and QTAIM atomistic insight. *Phys. Chem. Chem. Phys.* **16**, 3715-3725 (2014).
53. Zoete V., Meuwly M. Double proton transfer in the isolated and DNA-embedded guanine-cytosine base pair. *J. Chem. Phys.* **121**, 4377-4388 (2004).
54. Kimsey, I.J., Petzold, K., Sathyamoorthy, B., Stein, Z.W., & Al-Hashimi, H.M. Visualizing transient Watson-Crick-like mispairs in DNA and RNA duplexes. *Nature* **519**, 315-320 (2015).
55. Brovarets' O.O., Yurenko Y.P., Dubey I.Ya., Hovorun D.M. Can DNA-binding proteins of replisome tautomerize nucleotide bases? *Ab initio* model study. *J. Biomol. Struct. & Dynam.* **29**, 1101–1109 (2012).
56. Brovarets', O.O., & Hovorun, D.M. Can tautomerisation of the A·T Watson-Crick base pair *via* double proton transfer provoke point mutations during DNA replication? A comprehensive QM and QTAIM analysis. *J. Biomol. Struct. & Dynam.* **32**, 127-154 (2014).
57. Brovarets', O.O., & Hovorun, D.M. Why the tautomerization of the G·C Watson–Crick base pair *via* the DPT does not cause point mutations during DNA replication? QM and QTAIM comprehensive analysis. *J. Biomol. Struct. & Dynam.* **32**, 1474-1499 (2014).